Raman Spectroscopy and X-Ray Diffraction Studies of Zinc Oxide grown by Pulsed Laser Deposition

A thesis for the Degree of

Master of Science

Submitted to

Dublin City University

By

Sarah Byrne BSc.

Research Supervisor

Dr. Enda McGlynn

School of Physical Sciences

Dublin City University

January 2003

Declaration

I hereby certify that this material, which I now submit for assessment on the programme of study leading to the award of Master of Science is entirely my own work and has not been taken from the work of others save and to the extent that such work has been cited and acknowledged within the text of my work.

Signed: Sarah Byrne

Sarah Byrne

ID No.: 96504757

Date: 15/01/03

Contents

Figures and Tables

List of Figures

List of Tables

Acknowledgements

I would like to thank my supervisor, Dr. Enda McGlynn, and Prof. Martin Henry, Dr. Chaitali Roy and Dr. Jean Paul Mosnier for their help and encouragement and advice throughout the course of my studies.

Many thanks also to Eduardo DePosada and Donagh O'Mahony in the Laser and Plasma Applications group in Trinity College for growing the ZnO thin films and carrying out the XRD measurements.

Thanks, also, to everybody else who has given me his or her time and advice during the last two years.

Abstract

This work reports on the results of a spectroscopic study of Zinc Oxide (ZnO) and manganese doped Zinc Oxide ($Zn_{0.87}Mn_{0.13}O$). The samples were grown using Pulsed Laser Deposition (PLD) and were analysed as a function of their anneal conditions.

As a wide band gap semiconductor, ZnO, when grown to high quality, has the potential to be used in the fabrication of short wavelength devices i.e. LED's, laser diodes and lasers. In order to investigate the quality of the samples X-ray diffraction (XRD) and Raman spectroscopy were employed. These tools gave insight into the crystal structure quality, including the grain size, the lattice parameters and the presence of surface electric fields. The two probing techniques, Raman spectroscopy and X-ray diffraction, complemented each other well and there was a good correlation between the results they produced.

A preliminary study of $Zn_{0.87}Mn_{0.13}O$ was also carried out using Raman and XRD. The material grown was shown to be of reasonable quality. Since Mn doping increases the bandgap of ZnO, $Zn_{(1-x)}Mn_xO$, has the potential to emit even shorter wavelength radiation. Transition metal doped semiconductors are also being investigated for use in the area of Spintronics. $Zn_{(1-x)}Mn_xO$ is not yet widely studied so there is scope for further fundamental Raman spectroscopy studies.

A paper containing the non-resonant Raman and XRD results of the zinc oxide samples has been submitted to the journal Thin Solid Films.

Chapter 1: Introduction

1.1 Introduction

This thesis is concerned with the structural properties of zinc oxide (ZnO) as interpreted by Raman spectroscopy and X-ray diffraction with a brief look at manganese doped zinc oxide ($Zn_{0.87}Mn_{0.13}O$). Following in this introductory chapter are some interesting facts about ZnO and its origins, why it's being studied by numerous groups around the world, and the 'everyday' products and materials that it can be found in.

1.1.1 A Brief History of ZnO and ZnMnO

Zinc oxide has been known as a compound for at least 200 years and zinc itself identified as an individual element in Germany by the 16th century.[1] ZnO usually appears in the form of a white powder. It is still used in a huge number of areas and different grades of it are used depending on the application. In the early 1800's ZnO white was used to replace the lead white that was used in watercolour and oil paints since its white was 'whiter', it retained its whiteness for longer and it was less toxic than lead. It is still used in paints and glazes today for similar reasons.[2] In the rubber industry ZnO is used in the vulcanisation process of the rubber and also gives rubber a harder wearing finish and strengthens the compound against heat.[2] In terms of direct human consumption it is used in zinc supplement capsules and in sunblock lotions as it absorbs the harmful UV radiation from the sun. ZnO can also be found in plastics, pharmaceuticals and many more industries.[2] From a scientific view point the first Scanning Transmission Electron Microscope (STEM) image that was taken was of a ZnO single crystal in 1938.[2]

1.1.2 ZnO and $Zn_{(1-x)}Mn_xO$ as Semiconductors

Having briefly covered some of it's broader applications, ZnO will be re-introduced in this paragraph as a semiconductor. It has been studied for at least a century but not always in single crystal form. It was not until about the 1960's that serious spectroscopic investigations of semiconductor compounds took off. This was probably due to the influence of the LASER on spectroscopy in terms of light coherence and power. Also, as other semiconductors like silicon (Si) were being studied intently, there was a race on to see if another material would pose serious competition to Si. Therefore, there was a lot of fundamental research carried out in these decades (50's 60's) on all semiconductors including the II-VI compounds.[3] After this initial burst there has been a steady interest in all these materials but within the last decade there has been a surge of interest in ZnO due to it's potential as a UV emitter.

ZnO, along with gallium nitride (GaN), have the necessary properties for UV emission but ZnO has some distinct advantages over all of its colleagues. It has a large exciton binding energy at room temperature of 60meV (GaN is 28meV), which means that it should be a more efficient UV emitter and, hence, has a lower pumping power for inducing lasing than GaN.[4] Compared with the rest of the II-VI family, ZnO is considered one of the hardest materials and is, therefore, less likely to form dislocations or degrade over time. Last but not least it is easy to create very large n-type doping levels in ZnO as it has a high donor level concentration upon growth. For practical applications ZnO is available in large size wafers and can be grown in homoepitaxial layers unlike GaN. ZnO is also amenable to a variety of growth methods that GaN cannot avail of due to the very low melting point of Ga.[5]

The main disadvantage of ZnO in UV technology is that in order to produce a UV laser emitter from ZnO, a p-n junction must be built. However, there have been many problems in achieving this as ZnO films are intrinsically n-type. P-type films have been grown but only with very low hole concentration. Recently groups have

been trying to co-dope II-VI materials (e.g. adding in 2 acceptors levels for every donor) in order to achieve high acceptor concentrations.[6] This is done using Electron Cyclotron Resonance with an N_2O plasma. P-type ZnO has also been demonstrated with ZnO grown by reactive sputtering [7] and Molecular Beam epitaxy.[8]

Apart from its potential as a powerful UV emitter, ZnO is also used in varistors due to its wide bandgap and can also be used in gas sensing.[9] In the area of transparent conducting electrodes, ZnO has excellent properties – it has high optical transmittance in the visible region and good electrical conductivity. The range of wavelengths transmitted can be increased to include the blue/green region of the spectrum by doping with aluminium (Al) or gallium (Ga). Doping with Al also increases its conductivity. Transparent conducting electrodes are used in plasma display panels, solar cells and much more.[10] Finally ZnO has been widely used in Surface Acoustic Wave (SAW) devices. SAW devices are a branch of Guided Wave Acousto-Optics. The SAW technology is based on acoustic waves that are generated and contained to a certain depth (a fraction of a wavelength) in the surface of a material where they are controlled. It is the piezoelectric property of ZnO that allows the surface acoustic waves to be generated.[11]

One of the main features that doping of II-VI compounds with transition metals causes, is an increase of the lattice parameters of the compound and of the band gap [12] with increasing level of dopant. This could open the doors for creating different wavelength UV devices- as a wider band gap means smaller wavelength emission. $Zn_{0.18}Mg_{0.82}O$ films have been shown to have a bandgap as large as 6.7 eV.[13]

Although magnetic semiconductors were studied in the 60's and 70's there has been little attention paid to these types of material until very recent years with the advent of Diluted Magnetic Semiconductors (DMSs).[14] The main idea or incentive for studying these is to speed up computer processing in the areas known as Spintronics and Quantum Computing. Until now, most of this type of work has been restricted as none of the magnetic semiconductor materials could reasonably be integrated with the more popular semiconductor materials (i.e. Silicon). To date,

however, there have been no reports of ferromagnetic behaviour in ZnMnO either at low temperatures or room temperature.[15]

However, $Zn_{(1-x)}Mn_xO$ is only in its infancy compared with ZnO in terms of the amount of research carried out on it. UV emission from ZnO has been realised [16] and awaits full development. The possible applications of $Zn_{(1-x)}Mn_xO$ are, relatively, much further from this kind of development.

Having looked at a general overview of ZnO and $Zn_{(1-x)}Mn_xO$, the next section will deal with the practical problems of ZnO as a thin film in terms of growth methods, substrates, analysis techniques used and doping effects.

1.2 Growth and Characterisation Methods

The crystal structure of a material is of utmost importance if the material is to be applied successfully in electronic devices. In this case, for ZnO to perform lasing there would be a much higher chance of success the more 'perfect' the crystal is. Hence, the growth method and conditions are very important. The different changeable parameters of any growth method (i.e. temperature, pressure, substrate, time etc.) can all have profound effects on the resulting crystal structure and quality.

In this section we will begin by looking at the various growth techniques that have been employed to grow ZnO and $Zn_{(1-x)}Mn_xO$.

A study of the ZnO literature will yield the following kinds of popular growth methods: Pulsed Laser Deposition (PLD), Reactive sputtering, Electron Cyclotron Reduction, thermal oxidation of ZnS films, Molecular Beam Epitaxy (MBE) and many more.[17] In any of these methods there are a high number of growth parameters that affect the quality of the final film. Also, whether or not the film is going to be doped is also considered when choosing a growth method. Each method has its own

advantages and disadvantages. These are discussed in detail in Chapter 2 with relation to PLD – being the chosen growth method for the ZnO samples studied here.

In PLD, the target composition and material can also affect the resulting thin film. In PLD usually sintered ceramic ZnO and ZnMnO targets or metal Zn targets are used for ablation.

The most popular substrates used for ZnO growth are silicon (Si), forms of silica (SiO_2) and sapphire (Al_2O_3), and different types of glasses and quartz to name a few. The choice of substrate depends on a number of factors including growth method as discussed in chapter 2. ZnO is often used as a buffer layer for GaN growth due to their close lattice match.[18] Finally another main point to remember when choosing substrates is the application of the films – i.e. what type of spectroscopy is going to be used to characterise them and will the substrate effect it.

This leads nicely to the types of analysis techniques used to characterise these thin films. XRD would be the main one as it is readily available in most universities and research centres around the world. It also gives very fundamental information about crystal orientation and a good indication of the structural quality, grain size and lattice parameters. Photoluminescence (PL) and PL Excitation (PLE) are also widely used and can tell a lot about the optical properties and band gap structure of a semiconductor. X-ray photoelectron spectroscopy (XPS) and Energy Dispersive Spectroscopy (EDS) can give information on composition and identify impurities in thin films. Raman spectroscopy, which is used in this work, gives information on crystal structure, carrier concentration and structural quality of the thin film.[19] Raman scattering as a method will be discussed more thoroughly in the next section.

1.3 Raman Spectroscopy

So why use Raman spectroscopy as a characterisation tool? What are its advantages?

Firstly, by changing the laser wavelength different information can be extracted from a Raman Spectrum depending on a material's electronic transitions. Within reason, using different light sources does not have a great impact in the Raman spectra as only a 'difference' and not quantitative amounts is being plotted, that is, a frequency shift and not frequency is measured in a Raman Spectrum. However, in semiconductors, if the probing wavelength used is equal to or smaller than the bandgap of the material under investigation, then the result will be a Resonance Raman spectrum. In the case of ZnO the probing wavelength necessary for resonance Raman spectroscopy to occur is 380nm or less. Also, some samples may fluoresce at certain wavelengths and the fluorescence may be so intense that the Raman peaks become indistinguishable.

Raman spectroscopy is a non- invasive way of probing the crystal structure, phonon frequencies, composition and presence of free carriers and defects in a semiconductor. The laser power used in obtaining Raman spectra is also usually too low to damage the sample under observation.

There are many variations on the straightforward Raman spectroscopy. As mentioned above, resonance Raman occurs in semiconductors when the incident probing light has energy larger than the band gap and increases the sensitivity of certain modes. Microraman, like the system used to take the spectra in this report, uses a very small spot size and video equipment to focus on precise areas of the sample. Surface Enhanced Raman Spectroscopy (SERS), as the name suggests, takes spectra from the surface and consequently provides information on adsorbed particles. Also, using polarisers and analysers and changing the direction of incident probe light makes a Raman system extremely useful for more fundamental studies of materials.

Finally, a major advantage of Raman is that, when combined with Photoluminescence and Infrared spectroscopy, it covers almost all aspects of optical characterisation.[19], [20]

1.4 Project Aim

The main objectives of this work are to identify how and why PLD growth, and subsequent anneal conditions, affect the optical and structural properties of ZnO thin films. The ultimate goal is to optimise the growth conditions to create ZnO films that will emit UV laser radiation through optical pumping. As a minor project various types of doped ZnO (i.e. $Zn_{0.87}Mn_{0.13}O$) and fundamental variations in the PLD growth set up will be examined.

This work contributes to the ZnO study by examining samples with various growth and anneal conditions and subsequently narrowing down the growth options which lead to good quality films. In particular optimum anneal conditions are identified here for the particular growth temperature, chamber and oxygen pressure, substrate and target materials that were used in growing these ZnO samples.

This work also contains some preliminary measurements of $Zn_{0.87}Mn_{0.13}O$. The results of these may lead to further investigation in this area by our group.

The next chapter, Chapter 2, attempts to explain the necessary theoretical background of Pulsed Laser Deposition, X-Ray Diffraction and Raman spectroscopy while also giving a description of the experimental set-up used for each process.

Chapter 3 involves describing the precise growth and experimental conditions used in the PLD, XRD and Raman processes. The results and spectra of XRD and Raman spectroscopy are presented here also.

An interpretation of the results and their implications will be discussed in Chapter 4. The conclusions of all the work are presented in Chapter 5 along with suggestions for future work.

1.5 References

1. www.webelements.com
2. All information comes from various websites for example: www2.eng.cam.ac.uk/~bcb/history.html , www.jamesmbrown.co.uk/zno, www.studiomara.com/history , www.zochem.com
3. A.S. Grove, Physics and Technology of Semiconductor Devices, John Wiley & Sons. Inc., (1967)
4. www.cermetinc.com/cermet/projects/zno.html
5. www.compoundsemiconductor.net/magazine/article/8/7/2/2
6. S.B. Zhang, S.–H. Wei, Y. Yan, Physica B **302**, 135 (2001) X.-L. Guo, H. Tabata, T. Kawai, Optical Materials **19**, 229 (2002)
7. S. Tuzemen, G. Xiong, J. Wilkinson, B. Mischuck, K.B. Ucer, R.T. Williams, Physica B **308**, 1197 (2001)
8. H. Tabata, M. Sacki, S.L. Guo, J.H. Choi, T. Kawai, Physica B **308**, 993 (2001)
9. http://staff.ub.tu-berlin.de/~harloff/resint/engmat/znovar.html
10. G.A. Hirata, J. McKittrick, T. Cheeks, J.M. Siqueiros, J.A. Diaz, O. Contreras, O.A. Lopez, Thin Solid Films **288**, 29 (1996)
11. C.S. Tsai, Guided-Wave Acousto-Optics, Springer-Verlag (1990)
12. T. Fukumura, Z. Jin, A. Ohtomo, H. Koinuma, M. Kawasaki, Appl. Phys. Letts., **75**(21), 3366 (1999)
13. J. Narayan, A.K. Sharma, A. Kvit, C. Jin, J.F.Muth and O.W.Holland, Solid State Comms. **121** (1), 9 (2001)
14. H. Ohno, Science **281**, 951 (1998)
15. K. Ueda, H. Tabata, T. Kawai, Appl. Phys. Letts. **79**(7), 988 (2001)
16. M.H. Huang, S. Mao, H. Feick, H. Yan, Y. Wu, H. Kind, E. Weber, R. Russo, P. Yang, Science **292**, 1897 (2001) X. Guo, J. Choi, H. Tabata, T. Kawai, Jpn. J. Appl. Phys. **40**, L177 (2001)
17. For example: H.Z. Wu, K.M. He, D.J. Qiu, D.M. Huang J. Cryst. Growth **217**, 131 (2000), G.J. Exarhos, S.K. Sharma Thin Solid Films **270**, 27 (1995),

X.T. Zhang, Y.C. Liu, Z.Z. Zhi, J.Y. Zhang *et al.* J. Appl. Phys. D **34**, 3430 (2001)

18. R.F. Xiao, X.W. Sun, Z.F. Li, N. Cue, H.S. Kwok, Q.Z. Liu, S.S. Lau, J.Vac Sci. Technol. A **15**(4), 2207 (1997)
19. S. Perkovitz, Optical Characterization of Semiconductors: Infrared, Raman, and Photoluminescence Spectroscopy, Academic Press, (1993)
20. J.J. Laserna, Modern Techniques in Raman Spectroscopy, John Wiley & Sons Ltd., (1996)

Chapter 2: Experimental Techniques

2.1 Introduction

This chapter is intended to discuss why certain experimental methods were chosen by means of outlining the advantages and disadvantages of the techniques used. Then a description of the theory behind each of the methods is outlined. Finally the experimental set-up for each of the techniques is presented. Pulsed Laser Deposition will lead the discussion.

2.2 Pulsed Laser Deposition

Although it was first reported in 1965 by Smith and Turner [1], Pulsed Laser Deposition (PLD), has developed rapidly, mostly in the last 10-15 years. This is due to developments such as shorter Q-switch laser systems and the successful growth of different classes of materials (particularly superconductors) by various groups.[2] The slow development is surprising as PLD has many advantages over other more popular growth methods. These will be discussed below along with some of the disadvantages it also poses after a brief description of the theory behind pulsed laser deposition and the experimental set up.

2.2.1 Laser Ablation: A Theoretical Outline [2], [3], [4]

A laser plasma is created when a short laser pulse incident on a surface causes material to evaporate and so, form a plasma (a charged gas). The incident laser pulse causes local thermal heating at the target surface. This causes the irradiated area to melt and subsequently atoms, electrons and ions evaporate making the plasma.

The conditions for deposition of contents of the plasma plume on a substrate are :-

(i) the plasma density must not become too high as then it will screen the laser from reaching the target surface.

(ii) the laser power must be below a certain critical value which causes laser breakdown of the plasma (i.e. laser breakdown occurs when electrons in the plasma start absorbing the laser energy). The critical value is $<10^7$ Wcm^2.[3]

If a background gas is introduced into the plasma, or growth, chamber, the plume expansion will be slowed down and a shock front develops as can be seen in Figure 2.1.

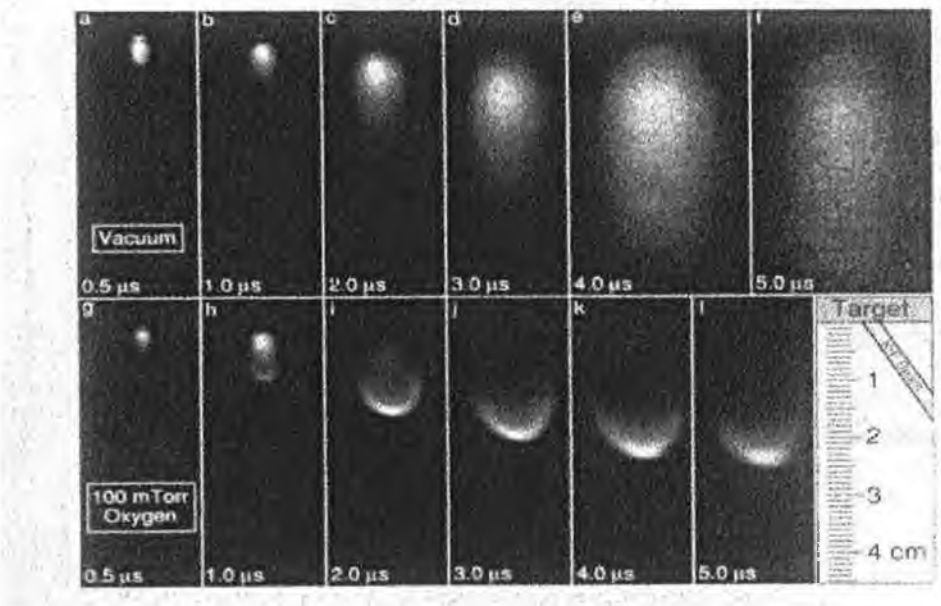

***Figure 2.1**: The top row of pictures shows the plasma plume expanding into vacuum with time. The bottom row shows the plasma plume expanding into a background gas.*[2]

Under these circumstances, the target-substrate distance would have to be carefully reconsidered as the shock front may prevent the right stoichiometry of material from reaching the substrate, or, may mean a decrease in the growth rate of the film as less material would be reaching the substrate per unit time.

2.2.2 Pulsed Laser Deposition Experimental Set-up

Figure 2.2 is a schematic of the PLD set-up used to grow the ZnO and $Zn_{0.87}Mn_{0.13}O$ samples studied here. This PLD system is based in the physics department of Trinity College, Dublin (University of Dublin). Eduardo DePosada, a member of the Laser and Plasma Applications group, grew the ZnO and $Zn_{0.87}Mn_{0.13}O$ using this system.

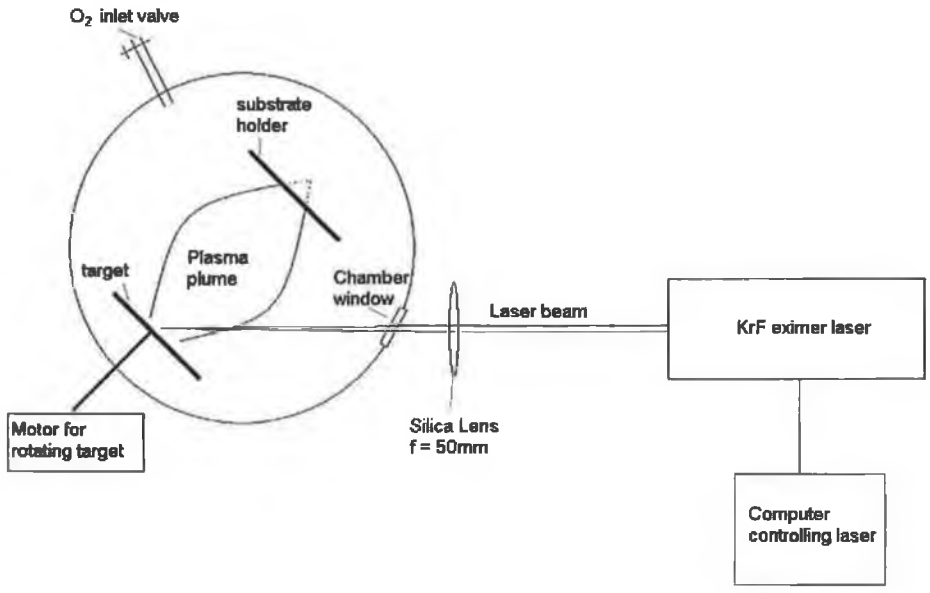

***Figure 2.2**: Diagram of the PLD system.*

The most important part of the set up is the laser. A KrF excimer laser (λ=248nm) was focussed by a silica lens (f=50mm) onto a target.

The chamber on the left of the diagram shows a target holder, substrate holder (heater), a window and a gas inlet pipe. Note: Diagram 2.2 is simplified – there would usually be more windows and gas inlet/outlet valves in any vacuum chamber

The target holder is rotated during growth by a small motor. The reason behind this is to prevent pitting in one area in particular, e.g. the laser may otherwise ablate one particular area that might be defective (e.g. zinc rich) in turn causing the film to be defective. For the growth of ZnO either a zinc or ZnO target may be used. However some other means of introducing oxygen into the film must be employed if a pure zinc target is chosen. PLD targets are usually made from pressed ZnO powder that has been sintered (baked in an oven) at extremely high temperatures to form a ceramic. Sometimes they are baked in an oxygen atmosphere to help maintain stoichiometry. If the target was made of softer material the laser pulse would just ablate a whole cluster of atoms from it and particulates would form in the film.

The substrate holder is directly opposite the target because the laser plume has a very narrow angular distribution. The laser is incident at an angle but the plasma is created in a forward direction so that the plasma deposits material on the substrate holder. Note also, that the substrate holder is usually a heater so that the substrate may be held at a certain temperature. When 'growth temperature' is referred to it actually means the temperature of the substrate holder.

The choice of substrate depends on a number of factors including growth method. For example, can the substrate withstand the growth temperature or pressure? In PLD, ZnO grown on Silicon (Si) experiences Si atoms diffusing into the ZnO thin film for temperatures above 400°C. The lattice match/mismatch is also a factor to be considered as the greater the mismatch the more likely there is to be dislocations in the thin film, although these may only become apparent above a critical film thickness. In ZnO particularly, the strains and stresses caused by lattice mismatches between film and substrate can induce an electric field due to ZnO's piezoelectric property. For the purposes of this work, sapphire was chosen due to its high temperature stability. It is this

characteristic which makes sapphire a very popular choice of substrate, even though sapphire and ZnO have quite a large lattice mismatch (~15%).

Also marked on the diagram is the manual inlet valve for gases, in this case for oxygen, O_2, as this is the background gas in the growth of ZnO. The introduction of oxygen gas helps maintain stoichiometery in ZnO.

2.2.3 Why Pulsed Laser Deposition? [2], [3], [4]

The pros and cons of using PLD as a growth technique are discussed below.

Advantages:

(i) The Laser used in PLD has advantages over other methods of growth in that it is easier to manipulate than a molecular beam, for instance.
Also, as the laser is the ablation tool, ablation is, to a large extent, independent of pressure as the laser-material interaction isn't greatly affected by the chamber pressure. Therefore ablation can occur at any deposition pressure giving PLD a greater pressure range than nearly any other deposition technique. The pressure in the chamber only effects the deposition on the substrate.

(ii) Almost all materials absorb the energy from laser light of less than 250nm so this makes any material a possible target for PLD provided a short wavelength laser is used. Therefore PLD can evaporate refractory materials. Other methods depend a lot more on the properties of the material.

(iii) Under the right conditions in PLD the stoichiometric composition of the target can be maintained but the right conditions are complicated to predict and so, are mainly found experimentally. Sputter deposition techniques however, can also maintain stoichiometric composition to high accuracy. Unfortunately, the plasma created by sputtering can also erode other materials apart from the target, adding impurities into the film being deposited.

(iv) Good Quality PLD films can be deposited at lower temperatures than in other popular thin film and bulk growth methods. This is because the energy the surface

atoms use to re-organise themselves and find their sites comes from the plasma itself as opposed to thermal energy from the substrate heater. The plasma enhances surface atom mobility by bombardment. However, if the energy of the incident atoms from the plume exceeds a certain limit then damage could be done to the layers that have already been deposited. Germanium (Ge) was grown on Ge using PLD at a substrate heater temperature of just 300°C which is less then half the 700°C needed for the same procedure to be done using Molecular Beam Epitaxy (MBE). PLD and MBE however will still use lower temperatures than other epitaxial growth methods such as Metal Organic Chemical Vapour Deposition (MOCVD).

(v) PLD is a relatively quick process i.e. it has a high deposition rate and a film of a few hundred nanometers in thickness can be grown in 15 minutes. MBE takes a lot longer but CVD is much faster.

(vi) In terms of semiconductor growth, PLD is much cheaper than methods such as MBE or MOCVD. PLD has particularly led to a revival in the study of II-VI semiconductors in the last 10 years.

(vii) Due to atomic layer by layer growth characteristics, PLD is useful for growing multilayered and nanoscale structures and has the potential for more complex uses, perhaps using screens and filters to grow more complex nano-devices which are possible with MBE. No other methods are capable of such controlled growth on a nanoscale level.

(viii) PLD is a much safer method than CVD or MOCVD as no volatile gases or materials are needed to create a chemical reaction.

Disadvantages:

(i) Particulate deposition is still a major problem area in PLD. Particulates are little molten lumps of the target that splash onto the substrate and solidify and cause disruption to the crystal lattice being formed. They occur when the laser energy is being transferred into heat energy quicker than it takes a layer of material of a thickness of half the skin depth to evaporate.[2] Careful control and tailoring of growth parameters are needed. In this case the laser characteristics and target

material are the most important to consider. Of course, for good quality growth of all types of crystal, all parameter change implications must be explored.

(ii) Another major disadvantage of PLD is that it is difficult to use for large area growth as the plasma plume only has a narrow angular distribution. This leads to non-uniform deposition over large areas. In this area, MOCVD and CVD are much superior because in large-scale production, they can grow large-scale homogeneous material at relatively high speeds.

2.3 X-Ray Diffraction

2.3.1 What we can Learn from XRD [5], [6]:

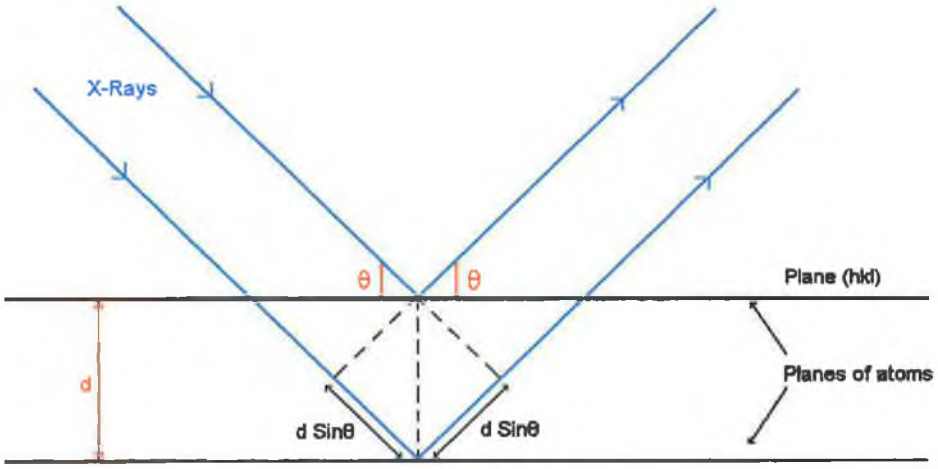

***Figure 2.3**: This figure shows a beam of x-rays incident on parallel crystal planes.*

X-Ray Diffraction, in θ-2θ mode, is based on the simple Bragg Law equation,

$$n\lambda = 2dSin\theta \qquad (2.1)$$

that describes X-ray reflection from the plane (hkl) and all parallel to it. θ is the angle the incident light makes with the (hkl) plane, d is the plane spacing of all planes parallel with Miller indices (hkl), λ is the wavelength of the incident radiation and n is the order of the reflection. These parameters are all labelled in figure 2.3.

Index determination of a crystal (i.e. assigning the peaks to sets crystal planes) can be carried out from an XRD pattern by following the basic rule that line positions determine the unit cell type and the relative shape and size of the line intensities determine the position of the atoms in the unit cell.

(i) Lattice Parameter Calculation [5]:

In order to determine the lattice parameters of the ZnO wurzite unit cell the simple plane spacing relation for a hexagonal unit cell is used. It is given as

$$\frac{1}{d} = \frac{4}{3}\left(\frac{h^2 + hk + k^2}{a^2}\right) + \frac{l^2}{c^2} \qquad (2.2)$$

combining this with Bragg's law, eqn. (2.1), gives:

$$Sin^2\theta = \frac{\lambda^2}{4}\left[\frac{4}{3}\left(\frac{h^2 + hk + k^2}{a^2}\right) + \frac{l^2}{c^2}\right]^2 \qquad (2.3)$$

where θ, λ and d are as in Braggs Law and a and c are the two axes used to define the hexagonal or the wurzite lattice. h,k and l are the Miller indices of the plane (hkl), or the index of the XRD peak in question.

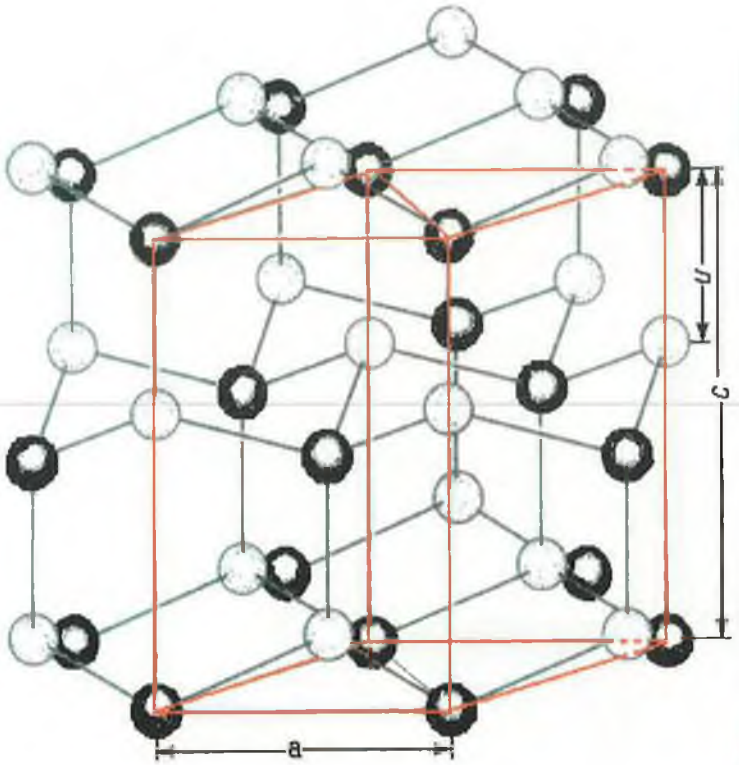

***Figure 2.4**: Wurzite structure of ZnO. (Reference 8)*

So as can be seen the lattice parameter c, is equal to d, the interplanar spacing of the (0001) planes. These parameters can be useful for comparison with bulk values to determine crystal quality and to look for any strain or stress in the crystal.

Figure 2.4 also shows the wurzite unit cell –it is outlined in red. The white atoms represent oxygen and the black ones, Zinc. A wurzite lattice is two hexagonal close pack lattices displaced vertically a distance u (as labelled in figure 2.4) from each other.

(iii) Grain Size Determination [5]:

As seen in the previous section, the Bragg Law can be used to calculate the distance between two planes and is designed to be used with a perfect crystal and a perfectly monochromatic and parallel beam of x-rays. The Scherrer relation, however, takes into account the whole thickness of the crystal, as well as x-ray diffraction line

broadening due to, for example, crystal and x-ray beam imperfections and finite grain size by incorporating the line's full width at half maximum (FWHM).

To calculate the average grain sizes of the samples, the Scherrer Relation is used. It is given by:

$$t = \frac{0.9\lambda}{BCos\theta} \qquad (2.4)$$

B is the full width at half maximum of the 2θ XRD line in radians, θ is the position of the line (half the 2θ value), λ is the wavelength of the incident x-rays and t is the average diameter of the crystal particle or grain.

It is important to note that the FWHM of the line being used should be the FWHM due to the grain size effect alone. Broadening due to the instrument and other factors (beam divergence etc.) should be taken into account. For this the FWHM of the single crystal, which should be ~ 0 for a perfect single crystal, should be subtracted using Warren's Method. This method is simply [5]:

$$B^2 = B_s^2 - B_{sc}^2 \qquad (2.5)$$

Where B_s is the FWHM of the line taken from the sample and B_{sc} is the FWHM of the same line taken from the single crystal.

2.3.2 Experimental Set-up for X-Ray Diffraction

The XRD spectra reported in this work were obtained with a Siemens Diffrac D500 diffractometer. The measurements were carried out in powder diffraction mode. A copper anode target is used and a Ni filter is in place so that only the Cu K-alpha X-Ray line is used for the diffraction.

These XRD measurements were performed in Trinity College Dublin, by Donagh O'Mahony of the Laser Plasma and Applications group.

2.4 Raman Spectroscopy and System

2.4.1 Introduction [7]

When monochromatic light is scattered from a surface 99.99% [7] of it will be elastically scattered – i.e. it will have the same wavelength upon scattering. This is known as Rayleigh Scattering. It is considered elastic scattering because there is no net energy transfer between the incident photons and the lattice vibrations.

However, the rest of the light has an increased or decreased wavelength upon scattering due to interactions with crystal excitations such as phonons. This small amount occurs from Raman and Brillouin scattering. Brillouin scattering occurs when the phonon that the incident light interacts with is acoustic. The process is called Raman scattering when the phonon emitted or absorbed is optical (For the purposes of this section Brillouin scattering is ignored). Raman Scattering can be considered inelastic scattering as the reflected light has either gained or lost energy to phonons in the crystal lattice under observation.

A Raman spectrum consists of a series of lines whose position corresponds to a frequency difference between the incident and scattered light (i.e. to a phonon mode of the crystal)

$$\text{i.e. } \Delta\nu = \nu_{Incident} - \nu_{scattered} = \nu_{phonon} \qquad (2.6)$$

versus the intensity of light scattered at that frequency.

An example of a complete Raman spectra:

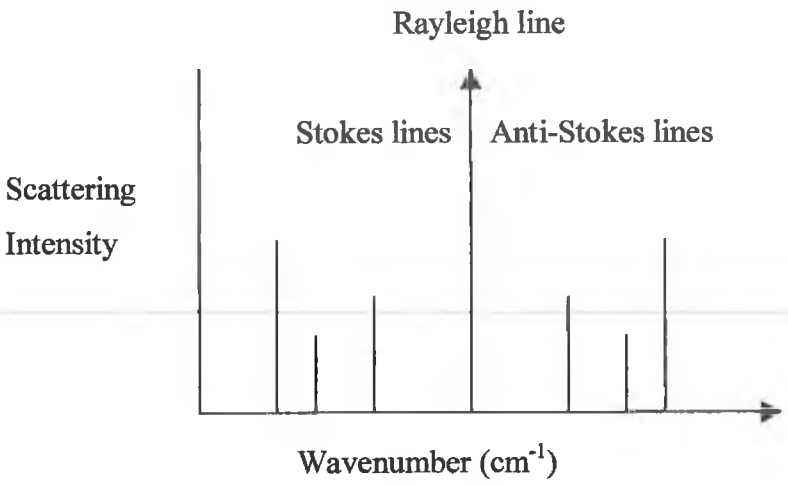

***Figure 2.5**: Basic diagram to show Stokes and anti-Stokes scatter.*

In figure 2.5, a feature in a Raman spectrum is considered Stokes shifted when the incident light loses energy so that a longer wavelength is scattered. When energy is gained by the photons the spectrum is called anti-Stokes shifted.

2.4.2 General Raman Theory[7], [10], [11]

An outline of the Classical Raman effect and Quantum Raman effect follows.

(i) Classical Treatment:

The condition for vibrational Raman Spectroscopy is that the amplitude of the dipole moment induced by the E-field of the incident radiation must change during the vibration. i.e. the polarisability of the molecule should change as it vibrates.

The relationship between the induced dipole moment and the polarisability is:

$$|\vec{\mu}| = \alpha|\vec{E}| \qquad (2.7)$$

where $|\vec{E}|$ is the electric field component of the incident radiation. So as the E-field interacts with the molecule, a dipole moment is induced and light is scattered at the same frequency as the incident light i.e. Rayleigh scattering

The oscillating electric field is given by

$$E = E_0 Cos 2\pi\nu_o t \qquad (2.8)$$

where E_o is the amplitude, ν_o is the frequency of the incident light and t is time.

and since $\mu = \alpha E$,

we can write $\mu = \alpha E_o Cos 2\pi\nu_o t \qquad (2.9)$

For the case of anisotropic molecules, polarisibility, α, is a tensor since polarisation along each axis of the lattice or molecule is different.

$$\begin{pmatrix} \mu_x \\ \mu_y \\ \mu_z \end{pmatrix} = \begin{bmatrix} \alpha_{xx} & \alpha_{xy} & \alpha_{xz} \\ \alpha_{yx} & \alpha_{yy} & \alpha_{yz} \\ \alpha_{zx} & \alpha_{zy} & \alpha_{zz} \end{bmatrix} \bullet \begin{pmatrix} E_x \\ E_y \\ E_z \end{pmatrix} \qquad (2.10)$$

A common way of expressing this is as the polarisibility ellipsoid (in this case the polarisibility coefficients are inversely proportional to the co-ordinate axes but there are other forms of this equation):

$$\alpha_{xx}x^2 + \alpha_{yy}y^2 + \alpha_{zz}z^2 + 2\alpha_{xy}xy + 2\alpha_{yz}yz + 2\alpha_{zx}zx = 1 \qquad (2.11)$$

where x, y and z are the principal axes of the ellipsoid.

So in order for the vibrational Raman condition to be satisfied the polarisibility must change with vibration i.e. with the vibrational co-ordinate, r:

$$\alpha = \alpha_o + \left(\frac{\partial\alpha}{\partial r}\right)_0 r \qquad (2.12)$$

where the vibrational co-ordinate, r, is related to the lattice vibration frequency, ν_p, by:

$$r = r_0 Cos(2\pi\nu_p t) \qquad (2.13)$$

A more detailed derivation would lead to second and third order terms in equation (2.12) which correspond to the second and third order Raman Scattering, however the intensities of these effects are usually small compared with the first order effects.
By substituting equations (2.8), (2.12) and (2.13), into equation (2.9) and rearranging the Raman effect can be shown to be:

$$\mu = \alpha_0 E_0 Cos2\pi\nu t + \frac{r_0 E_0}{2}\left(\frac{\partial\alpha}{\partial r}\right)\left[Cos2\pi(\nu - \nu_p)t + Cos2\pi(\nu + \nu_p)t\right] \quad (2.14)$$

where, on the right hand side of the equality sign, the first term is equivalent to Rayleigh scattering and the second term takes into account the changing polarisibility to account for both Stokes and anti-Stokes Raman scatter.

(ii) Quantum Treatment of the Raman Effect

The main assumption behind the Quantum treatment is that vibrations of a system of atoms in a molecule are described as a harmonic oscillator. When radiation interacts with crystal vibrations, a *discrete* amount of energy is lost or gained from the photon energy i.e. $h\nu \pm \Delta E$. This discrete packet of energy is called a phonon. It is considered that there are different vibrational energy levels and the energy difference between a transition corresponds to the frequency shifts in the Raman spectrum.

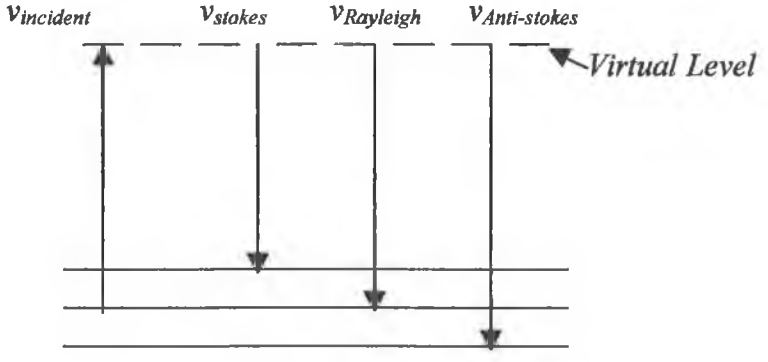

***Figure 2.6**: Quantum treatment of Raman scattering.*

Since most optical vibrational modes will be in their ground state at room temperature before any interaction with photons, then Stokes' scattering is more likely. From a quantum mechanical treatment the Stokes' spectra will be more intense than the anti-Stokes' as the transition probability is higher for ground to first state transitions than higher states to ground states transitions. In the classical treatment there is no distinction between which, Stokes or anti-Stokes, interaction is most probable to occur. The quantum treatment agrees with experimental results, and the Stokes/ anti-Stokes ratio is actually used as a measure of crystal temperature. This is because thermal energy causes more vibrations to be in higher states and so anti-Stokes scattering becomes more intense, i.e., the smaller the Stokes/anti-Stokes ratio, the higher the crystal temperature.

2.4.3 Raman Spectroscopy of ZnO [10], [12], [13]

ZnO has the wurzite structure with C_{6v} symmetry. It is a polar uniaxial crystal and has no centre of inversion – therefore it has piezoelectric properties.

The wurzite lattice has 4 atoms per unit cell. The Raman Active zone centre phonon vibrations predicted are: one A_1 mode, one E_1 mode and two E_2 modes. (Group Theory also predicts two B_1 modes but these are silent.) The infrared active vibrations are the A_1 and E_1 modes. In wurzite ZnO long range electrostatic forces dominate over the short range interatomic forces. This leads to a split into longitudinal and transverse components of the phonon normal modes that are infrared active i.e. the A_1 and E_1 modes will be split. There will be $A_1(TO)$, $A_1(LO)$, $E_1(TO)$ and $E_1(LO)$ vibrational modes in the Raman spectrum of ZnO as well as the two E_2 modes(TO = Transverse Optical and LO = Longitudinal Optical). [10]

Many experiments have been carried out to distinguish which peak values correspond to which normal modes [c.f. Reference 11]. To do this, the incident radiation must be polarised, the direction of propagation of the incident light must be controlled and the scattered radiation must be analysed. However, in the experiments reported on in

this work unpolarised light was used and they were performed in the backscattering geometry.

Resonance Raman Scattering [9], [14]

Resonant enhancement of Raman spectra is a second order scattering Raman process. When the incident electromagnetic radiation corresponds with, or is close to, an electronic transition in the semiconductor (i.e. exciton transition) the probability of a transition becomes greater. Polaritons are considered to be the intermediary states. Only the LO modes, coupled to these transitions are enhanced.[9]

Resonance Raman Spectra are considerably simpler for this reason as can be seen from the resonance spectra shown in figure 3.2.

Impurities and Defects [9], [11]

The translational symmetry of a crystal is what defines a phonon. If impurities or defects break this translational symmetry, new modes can occur. Localised modes occur when their frequency is too large to propagate through the crystal like a normal phonon.[11] These modes can be known as band modes (non-localised) when the defect or impurity atom is heavier than the lattice atoms surrounding it. In a diatomic crystal, as in the case of ZnO and $Zn_{(1-x)}Mn_xO$ for small x, if a lighter atom replaces the heavier atom, localised modes and gap modes occur. Localised modes are ones whose frequencies occur higher than the perfect lattice frequencies i.e. all acoustic and optical modes. Gap modes have frequencies between bands of allowed modes – i.e. between the acoustic and optical modes in ZnO. Band modes occur within bands of perfect lattice frequencies i.e. between the TA and LA modes or between TO and LO modes.

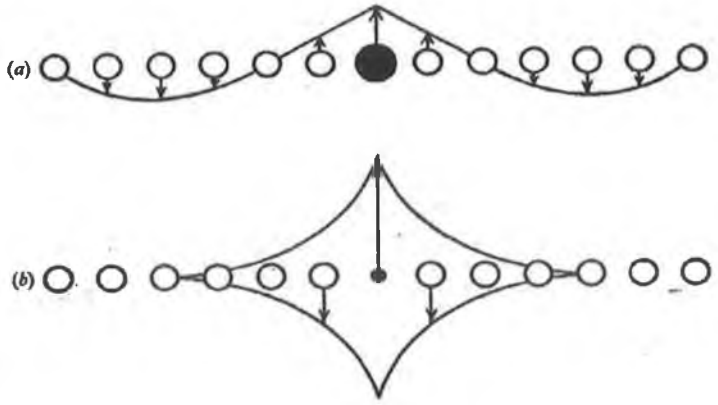

***Figure 2.7**: This figure shows (a) a non- localised mode where the vibration travels through the crystal (band mode) and (b) a localised mode (local mode or gap mode) where the vibration remains in the vicinity of the impurity atom.(Picture from ref. 9)*

2.4.4 The Raman Spectrometer

Raman spectrometers have changed dramatically due to the advent of lasers, semiconductor detectors and precision optics over the decades.

When designing a Raman spectrometer there are two main considerations:

(i) Raman scatter intensity is less than 1% of the Rayleigh scatter making it very weak and hard to distinguish.

(ii) The Raman shift is quite small and Raman peaks remain close to the main Rayleigh scatter line worsening the situation because the Raman signal lies on an intense background signal.

Taking these considerations into account means that all aspects of a Raman system must be of high quality and precision. Powerful light sources, sensitive detectors and accurate optic systems are necessary to enhance the clarity and resolution of a Raman spectrum.

2.4.4.1 The Typical Raman Spectrometer [7], [11]

The main equipment of a typical Raman spectrometer will now be discussed.

(i) The Optics

Figure 2.8 shows a typical Raman spectrometer set-up using 90° scattering geometry. The inset shows what a typical 180° backscattering system looks like.

Depending upon the intended material to be studied different scattering geometries are chosen. In the case of semiconductors the backscattering configuration is usually used. More often optic fibres are being used in Raman systems to carry the light signal from the sample to the spectrometer.

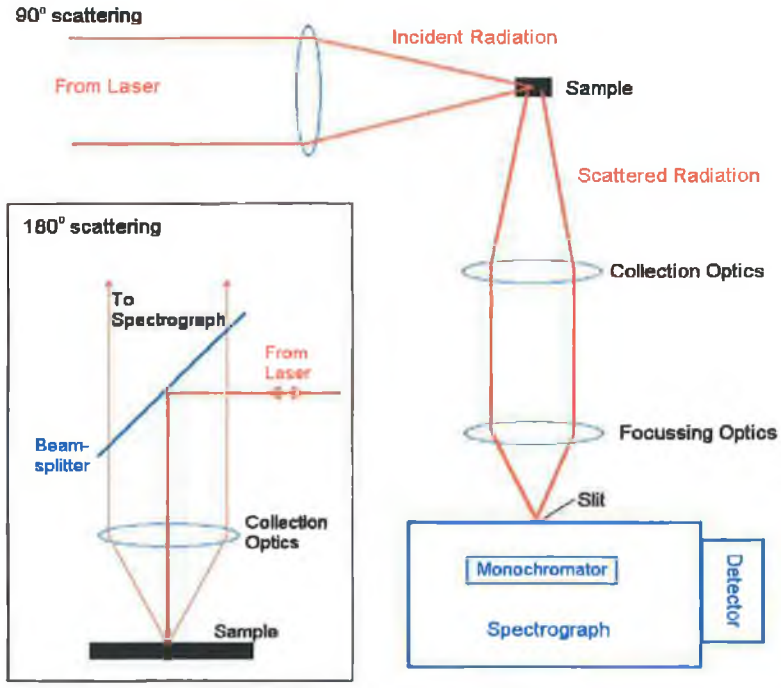

***Figure 2.8**: The main part shows a typical 90° scattering set-up. The inset shows a typical 180° backscattering set-up.*

(ii) The Laser

Very old Raman systems (i.e. before the introduction of the laser) normally used mercury arc lamps as an almost monochromatic source. The main mercury line is at 435.8nm but other weaker mercury lines had to be filtered out. Raman systems with these light sources needed larger volume samples in order to get a measurable intensity signal. Other disadvantages of mercury light sources are that only colourless liquids could be studied as even slightly yellowish liquids absorbed this line and solid samples were hard to illuminate.

The introduction of the laser eliminated most of these problems. With a laser Raman systems were able to use high power needed to make Raman signals stronger and completely monochromatic light which eliminated extra filters needed for mercury arc lamps. The most commonly used lasers in Raman systems are the He-Ne laser, and both the Ar+ and Kr+ ion lasers. All three are continuous emission lasers. The Ar+ and the Kr+ lasers are favourable, as each one has a number of different wavelengths available for use. Generally Raman spectra should not be affected much by laser wavelength but if the wavelength corresponds to an electronic transition in a semiconductor then resonance enhancement can occur. Whether or not a sample will fluoresce with certain incident wavelengths is also a consideration for choosing a laser or probe wavelength. Detector response is also another factor to take into account.

(ii) Filters and Spectrographs

Factors to take into consideration for spectrographs are that stray light of the order of 10^{-10} of the incident laser light may only be transmitted so as not to obscure the Raman signal. The Raman signal being transmitted must be maximised and the dispersion in terms of how much spectral coverage will reach the detector must also be taken into account.

A single monochromator used in most spectroscopy systems is not sufficient for use in a Raman system as not enough of the stray light is rejected. However the

throughput of the Raman signal of a single monochromator is high compared with other options.

Most commonly used is the double monochromator which rejects ~10^{-10} of the Rayleigh light. Double monochromators act as tuneable bandpass filters with a variable bandpass width but their dispersion is larger than that of a single monochromator, which means they cannot be used efficiently with large flat detectors. Usually they are used with photomultiplier tubes and to get a whole spectral coverage involves multiple measurements.

Triple monochromators have excellent stray light rejection and lower dispersion but their main disadvantage is that they have low transmission intensities, which does not suit the weak Raman signal from most materials.

Another form of single monochromator, which is becoming more popular, is a holographic filter. These have excellent transmission, low dispersion and excellent Rayleigh light rejection. The only disadvantage is that they are made specific to the wavelength of the laser and so have to be replaced for every different wavelength used. These will be discussed in more detail in the next section on the Holoprobe Raman system.

(iii) Detectors

Originally photographic plates and cameras were used to record a Raman spectrum. The exposure time would range from minutes to hours. As mentioned above PM tubes, cooled to reduce noise contributions to the spectrum, were the most commonly used.

Nowadays multichannel detectors are becoming more common as a whole spectrum can be recorded at once. Diode array detectors are also popular but the resolution of the spectrum can be compromised depending on the size of the diodes. CCD devices are at the forefront as they can record whole spectral range at once without loosing resolution. All detectors have to be cooled in some way to reduce noise from thermal excitations of electrons.

2.4.4.2 The Holoprobe Raman Spectrometer [15]

The Raman system that was used to obtain the spectra is now described. A diagram of the system is shown below in figure 2.9.

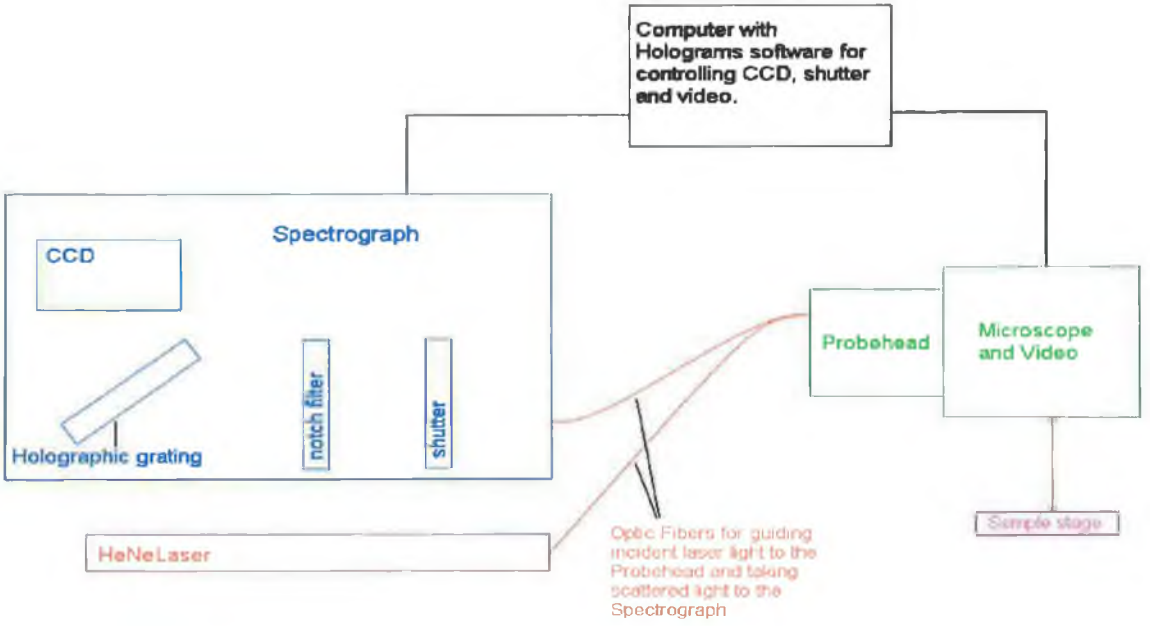

***Figure 2.9**: Diagram of the basic set up of the Raman System.*

Now some of the major parts of the system will be described in more detail.

(i) Laser and Optics: The Holoprobe Head and Microscope

Figure 2.10 is a diagram of the probe head. The notch filters here are used to eliminate the contribution from the silica Raman spectra generated when the light passes through the optical fibres. They are also used to partly eliminate Rayleigh scatter on the return signal.

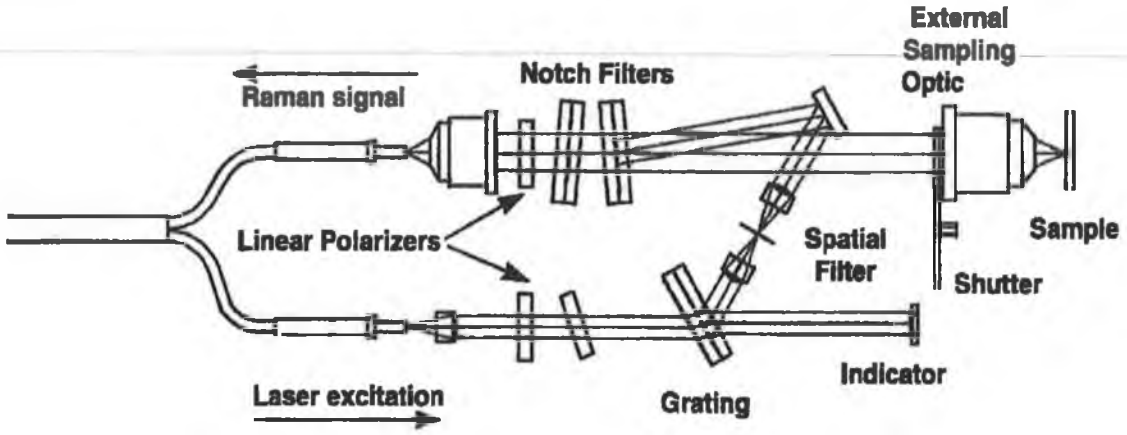

***Figure 2.10**: The probehead. (Reference 15)*

The light travels from the laser to the probe head via optical fibre and the scattered light from the sample is also transported to the spectrograph from the probe head. This is done using optical fibre connections shown in figure 2.12.

The central fibre is from the laser, the excitation fibre, and the other fibres around it collect the light for analysis. The laser beam is incident on the sample through the microscope lens objective. The scattered light is also collected through the objective. There is a small video camera installed in the microscope and this is used so that one can focus clearly using the picture from the video on the computer to see what part of the samples to focus the excitation beam on.

(ii) The Filters and Spectrograph

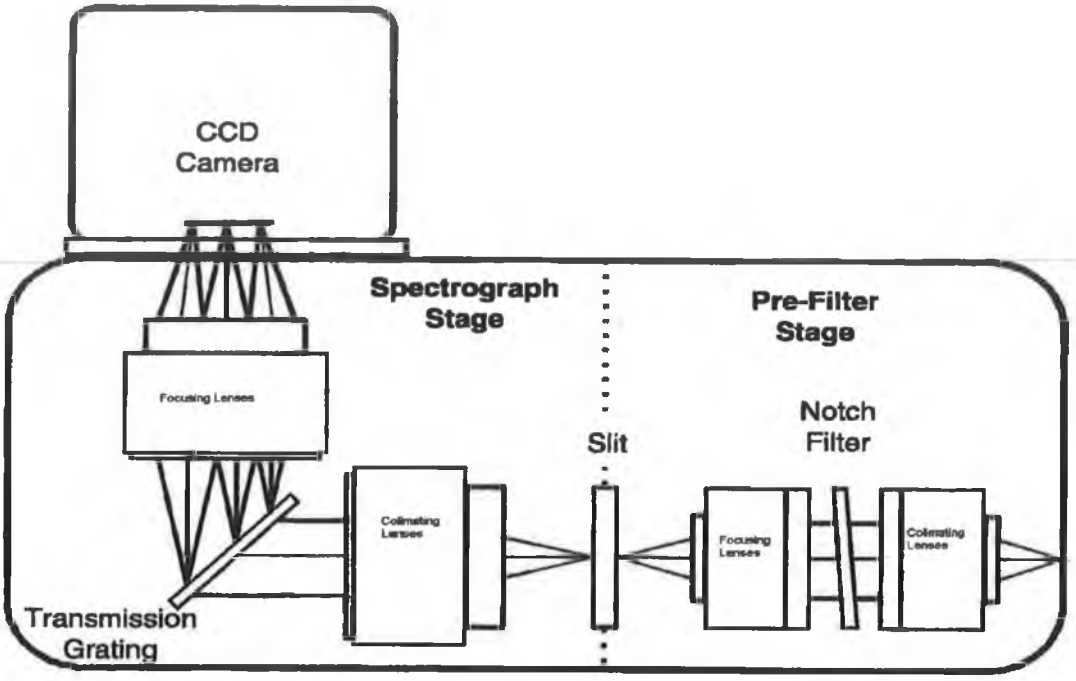

***Figure 2.11**: This figure shows a schematic of the Spectrograph. (Reference 15)*

The most important feature in the spectrograph is the holographic transmission grating and filter. These holographic optics are collectively know as Volume Phase Holograms (VPH). The VPH transmission gratings are period refractive index gradients. These periodic arrays diffract light in a volume or Bragg style as opposed to conventional ones, which diffract in the surface regime. The diffraction efficiency is greater than 80% and the transmission efficiency of the VPH's is greater than 90%. Since these holographic optics are generated from dichromated gelatin (DCG) they are best in use in the Visible or near infrared wavelengths so the HeNe fits this category perfectly.

The transmission grating and the notch filter (used for blocking out the Rayleigh scatter) are labelled in the diagram. The sets of lenses on either side of the grating are

In conclusion, the main advantage of the Holoprobe system is that the Holoplex gratings allow a huge spectral region to be examined at once unlike more conventional gratings. Although the holographic notch filters have excellent rejection of Rayleigh scatter, the very minimum they can allow measurements is to within $50cm^{-1}$ of the Rayleigh line – this is where triple monochromators would out-perform them. The CCD camera used for detection of the Raman scattered light can measure, in one acquisition, the greatest scattered wavelength range compared to the other methods described in 2.4.4.1. The spectral resolution of the spectra obtained with a Raman microprobe is of the order of a couple of wavenumbers.

2.5 References

1. H.M. Smith, A.F. Turner, Appl. Optics **4**, 147 (1965)
2. D.B. Chrisey, G.K. Hubler, Pulsed Laser Deposition of Thin Films, John Wiley& sons (1994)
3. B.M. Smirnov, Physics of Ioinized Gases, John Wiley & sons (2001)
4. P.R. Willmott and J.R. Huber, RPM Colloquia, Reviews of Modern Physics **72**(1), 315 (2000)
5. B.D. Cullity, Elements of x-ray diffraction, Adison-Wesley publishing company Inc. (1978)
6. N.W. Ashcroft, N.D. Mermin, Solid State Physics, New York : Holt, Rinehart and Winston (1976)
7. Banwell, McCash, Fundamentals of Molecular Spectroscopy 4th Edition, McGraw-Hill Book Co. (1994)

   B.P. Straughan, S. Walker, Spectroscopy (2), Chapman and Hall, Science Parperbacks (1976)

   J.J. Laserna, Modern Techniques in Raman Spectroscopy, John Wiley & Sons (1996)

8. K.-H. Hellwege (Ed), Numerical Data and Functional Relationships in Science and Technology, Group III: Crystal and Solid State Physics, Volume **17b**, Physics of II-VI and I-VII Compounds, Semimagnetic Semiconductors, Springer-Verlag (1982)
9. P.M.A. Sherwood, Vibrational Spectroscopy of Solids, Cambridge University Press (1972)
10. R. Loudon, Advan. Physics **10**, 908 (1955)
11. S. Perkowitz, Optical characterisation of Semiconductors, Academic Press Ltd. (1993)
12. T.C. Damen, S.P.S. Porto and B. Tell, Phys. Rev. **142**, 570 (1966)
13. C.A. Arguello, D.L. Rousseau, S.P.S. Porto, Phys. Rev. **181**(3), 1351 (1969)
14. R.C.C. Leite, J.F Scott, T.C. Damen, Phys. Rev. Lett. **22**(15), 780 (1969)
15. Holoprobe Operations Manual, Kaiser Optical Systems (1997)

Chapter 3: Experimental Data

3.1 Introduction

In this chapter the precise growth conditions of the samples studied, ZnO and $Zn_{0.87}Mn_{0.13}O$, will be described. Following that, the Raman and XRD spectra of both sets of samples will be presented and their main features will be highlighted ready for discussion in Chapter 4.

3.2 Precise Growth Conditions

3.2.1 Zinc Oxide Samples:

Varying the anneal conditions of the ZnO samples was chosen as being vitally important to study in order to obtain high quality ZnO. Numerous studies have been carried out on Pulsed Laser Deposited ZnO in the literature.[1] From these results average growth conditions were chosen as a starting point for the growth of good quality ZnO.

The ZnO samples were all grown under the same laser parameters, background gas pressure and substrate temperature conditions but they were annealed at various temperatures.

The experimental set-up was as shown in figure 2.1. Firstly, a molecular pump pumps the growth chamber down to a 10^{-6} mbar base pressure. Then oxygen (99.999% purity) is introduced into the chamber until the pressure increases to the desired value. An O_2 partial pressure of 0.3 mbar was used for the ZnO growth.

The laser used for ablation is an Eximer KrF laser with a wavelength of 248nm and pulse duration of 26ns. It is focussed through a Silica lens (f = 50mm) to a spot size

of 6x1mm on the target. The laser energy per unit area or fluence on the target is 1.7 J/cm^2 and the repetition rate of the laser is 10 Hz.

The substrate and target were at a distance of 4 cm apart for the growth of all samples. The target was a ZnO ceramic disk (99.99% purity) and the substrate used was (0001) surface of α-Al_2O_3. The substrate was attached to the substrate heater using vacuum compatible silver paint and the target to the target holder using the same. The substrate temperature was maintained at 400^0C for all samples.

The ZnO films were then annealed in oxygen in the growth chamber directly after deposition at different temperatures and for different lengths of time. Table 3.1 contains the growth conditions for each ZnO sample.

Sample	Growth temp. (^{0}C)	Anneal temp. (^{0}C)	Anneal duration (mins)
a	400	no anneal	0
b	400	400	10
c	400	500	15
d	400	600	10

***Table 3.1**: Anneal temperatures and anneal times for ZnO growth.*

3.2.2 Manganese-doped Zinc Oxide Samples:

The same oxygen partial pressure, target-substrate distance and doping levels were maintained for the $Zn_{0.87}Mn_{0.13}O$ samples and so they were studied with respect to different growth temperature and anneal conditions. Varying growth temperature and anneal conditions were again chosen for the manganese samples to complement the previous ZnO study.

The $Zn_{0.87}Mn_{0.13}O$ samples were grown using the same system as the ZnO samples so in this section any parameters not mentioned can be assumed to be the same as in the previous section on ZnO growth conditions.

For the growth of $Zn_{0.87}Mn_{0.13}O$ a $Zn_{0.87}Mn_{0.13}O$ sintered disk was used as the target. The O_2 partial pressure was kept at 0.4 mbar for the growth of all samples. The

target-substrate distance was also maintained at ~4cm. The changing parameters during the $Zn_{0.87}Mn_{0.13}O$ sample growth were (i) substrate temperature and (ii) annealing conditions. All anneals were done in oxygen and at the various sample growth temperatures unless otherwise stated. The different conditions are listed in Table 3.2 below.

Sample	Growth Temp. (^{0}C)	Annealing time (mins)
g	250	no anneal
h	250	20
j	400	no anneal
k	400	20
l	400	20 /in vacuum
p	550	no anneal
q	550	20

***Table 3.2**: Growth temperatures and annealing conditions for the $Zn_{0.87}Mn_{0.13}O$ samples.*

3.3 Raman Spectroscopy Results

3.3.1 Experimental Conditions:

The Samples were placed on a slide under the microscope. The spectra were taken in air at room temperature using unpolarised HeNe excitation (λ=632.9nm) in the backscattering configuration. The crystallographic orientation of the thin films can be determined from the XRD results in section 3.4, therefore we know that the incident radiation was along the c-axis of the sample in the Raman scattering experiments.

As the samples are 5mmx5mm in size, the video mode was used to choose which parts of the sample to use for Raman spectroscopy. Some samples were very smooth and level and spectra from different parts were identical. Using the video, defects or damage on some sample surfaces were avoided. In all cases spectra were taken from numerous

different sites in order to validate the consistency of the spectra and hence, sample quality.

All Raman spectra were taken with the CCD camera at 233K (minimum temperature), for 30-second exposure at 3 accumulations with intensity and wavelength calibrations enabled and a new dark spectrum taken for each accumulation.

3.3.2 Zinc Oxide Raman Spectra

Figure 3.1 shows the non-resonant Raman spectra taken for the ZnO samples:

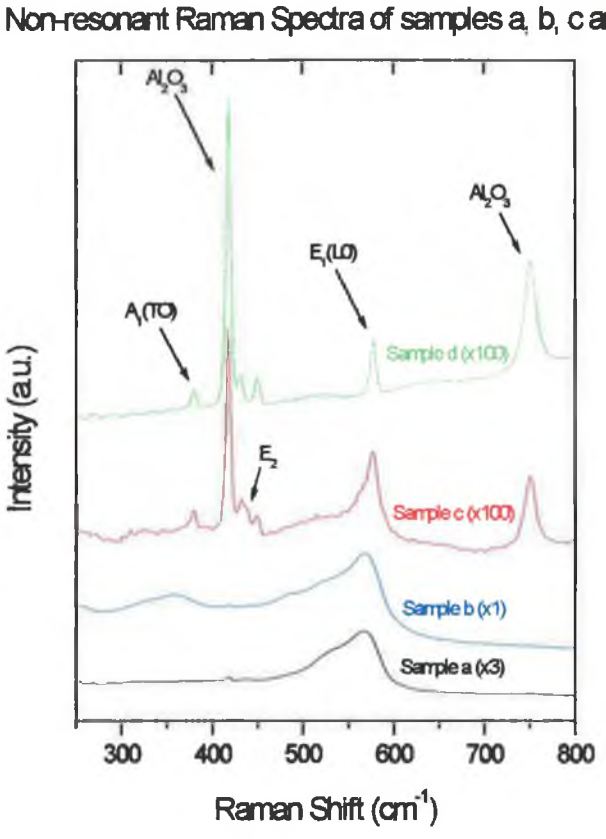

Figure 3.1: Raman Spectra of samples a,b,c and d.

Note: Samples a & b's spectra are of considerably higher intensity than the spectra for samples c & d. The sharp peak at 417cm^{-1} is from the Sapphire substrate and its intensity remains very similar in all samples and so can be used for comparison purposes.

As marked out on the graphs there are three ZnO modes visible in the Raman Spectra. These are the A_1(TO), the E_2 and the E_1(LO). The two peaks at 417 cm^{-1} and 750 cm^{-1} are from the sapphire substrate.

Two very comprehensive Raman studies of single crystal ZnO have been carried out by Damen, Porto and Tell [2] and Arguello et al.[3] Both groups explain the detailed polarised Raman experiments they used to determine the positions of the ZnO Raman peaks. Their results agree to within ±7 cm^{-1}. Below is a table of their results and the peaks that are seen in the unpolarised Spectra reported on here.

	E_2 (cm^{-1})	E_2 (cm^{-1})	A_1(LO) (cm^{-1})	E_1(LO) (cm^{-1})	A_1(TO) (cm^{-1})	E_1(TO) (cm^{-1})
Damen et al. (1965)[2]	101	437	574	583	380	407
Arguello et al. (1969)[3]	101	444	579	591	380	413
PLD ZnO samples	---	~437	---	567 to 577	380	---

***Table 3.3**: Comparison of reported Raman results and the results from the PLD grown ZnO samples.*

Unfortunately the overlapping sapphire peak at 417cm^{-1} means it is not possible to tell if the E_1(TO) peak, which is expected around 410cm^{-1}, exists but the symmetry of the sapphire peak suggests that if it is present it is of very low intensity. The A_1(LO) mode is not present as the incident light is along the z or c-axis and so is forbidden due to its selection rules (as discussed in the Raman theory section in chapter 2). The second E_2 mode is not present as the notch filter in the Holoprobe instrument will not transmit so close to the Rayleigh line.

Of the three modes visible in the spectra, the E_2 mode (437.5cm^{-1}) is present in samples *a*, *b* and *c*. The A_1(TO) mode (380cm^{-1}) is visible in samples *c* and *d*. The

E_1(LO) mode is the most prominent of all three and significantly reduces in intensity, asymmetry and FWHM with increasing annealing temperature. It also shifts from 567cm^{-1} to 577 cm^{-1} from sample *a* to *d* with increasing anneal temperature. However not all of the broad band that is seen in samples *a* and *b* is attributed to simply the E_1(LO) mode as will be discussed in the next chapter.

3.3.3 Resonance Raman Spectra:

Resonance spectra were also taken of the ZnO samples using UV excitation as shown in Fig. 3.2. A helium cadmium laser was used in the backscattering formation with a liquid nitrogen cooled CCD. The energy of the HeCd is 3.82eV and so it is larger than the electronic band gap of bulk ZnO which has a band gap band gap of ~3.3eV. This provides the necessary conditions for resonance spectra to be taken. Figure 3.2 below shows the resonance spectra for samples *a* and *c*. All LO modes are expected to be enhanced by Resonance excitation. If the incident radiation wavevector was perpendicular to the c-axis, it would be expected that the A_1(LO) mode would be enhanced instead of the E_1(LO), as is the case here. These spectra also show that the resonance spectra have more than one order of vibration. In Figure 3.2 the 2LO mode can be seen. Leite, Scott and Damen have seen all modes up to and including the 9LO mode in CdS [4].

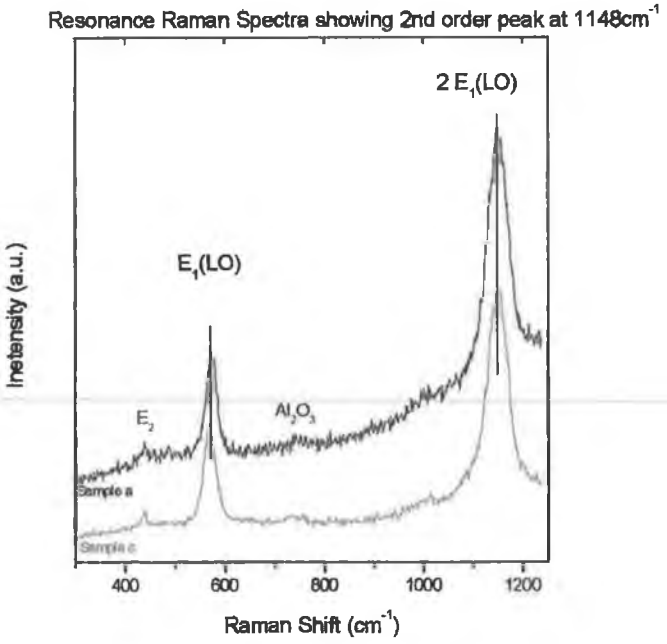

***Figure 3.2**: Resonant Raman Spectra of samples a and c.*

The peak at about 570cm^{-1} is the E_1(LO) mode. It has been enhanced by the UV excitation. The second large peak at 1148cm^{-1} is the second order peak of the same vibrational mode. The E_1(LO) mode is noticeably more symmetrical and is of the same intensity in samples which showed great differences in their non-resonant Raman spectra.

3.3.4 Manganese-doped Zinc Oxide Raman Spectra

The non-resonant Raman spectra for the $Zn_{0.87}Mn_{0.13}O$ samples were taken at an exposure time of 45 seconds and for 5 accumulations. All other Raman experimental conditions remained the same as for the ZnO samples. Figure 3.3 shows the spectra in the range 300cm^{-1} to 800cm^{-1}.

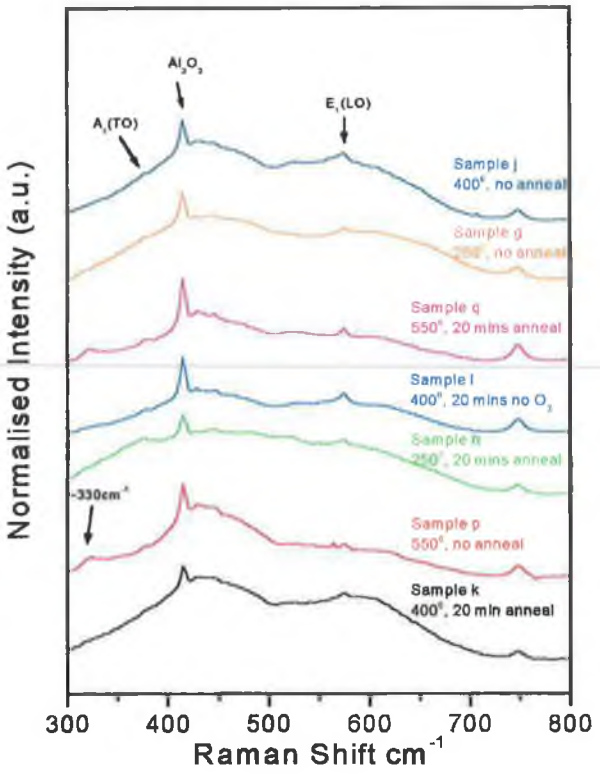

***Figure 3.3**: Raman Spectra of samples g,h,j,k,l,p and q.*

The peaks at 417cm^{-1} and 750 cm^{-1} are again due to the sapphire substrate. The ZnO E_1(LO) (577cm^{-1}) can be seen in all samples and is quite strong in all of them. The A_1(TO) mode at ~380cm^{-1} is present in most samples. In addition to these modes, there are two broad spectral features centred around ~435cm^{-1} and ~590cm^{-1}.

The main points of interest in these $Zn_{0.87}Mn_{0.13}O$ samples is that there is little change in their Raman spectra compared with a large change in their growth conditions, however, none of these samples were annealed at temperatures higher than their growth temperatures. The intensities of the spectra here are comparable with those of the annealed ZnO samples *c* and *d*. There is also consistent evidence of surface, local and band phonon modes as explained in more detail in the discussion.

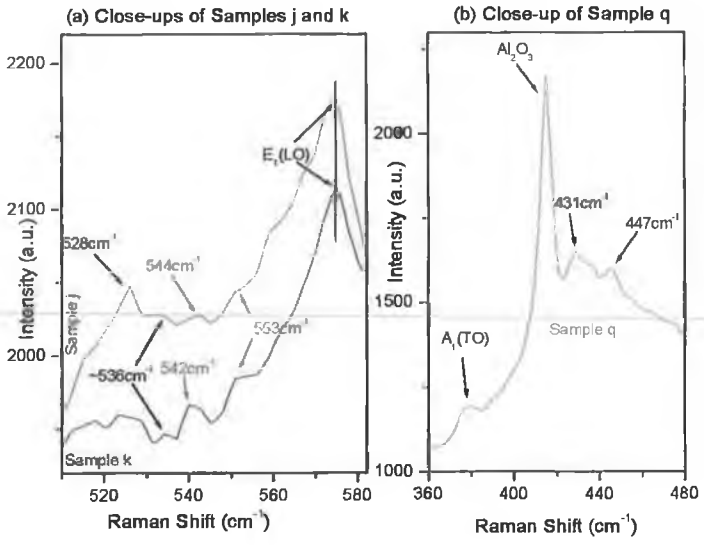

***Figure 3.4 (a) and (b)**: Close ups of Raman Spectra of l, k, and q.*

Surface ZnO modes have been calculated and reported by Ibach[5] to occur at 543cm^{-1} and 553cm^{-1}. As can be seen from the close-up of samples *j* and *k*, there is evidence of these modes at 542cm^{-1} & 544cm^{-1} and 553cm^{-1}. They are marked in red in fig 3.4 (a). It also appears in some other samples not shown in the close-up. In most samples there are a series of peaks between 510cm^{-1} and 570cm^{-1}, the range shown in fig 3.4 (a). Examples of these are a quite strong peak at 528cm^{-1} and a very weak but one that occurs in a few samples at 536cm^{-1}. These, and others like them, could be local, surface or band modes corresponding to ZnO or, mixed LO modes due to the different binary constituents, ZnO and MnO, which occur in the intermediate mode behaviour.[6]

Note: These spectra were taken for 45 seconds and for 5 accumulations with a new dark current being subtracted from each accumulation in order to reduce noise. It is believed, therefore that these small peaks are not due to noise. They are repeatedly obtained scan to scan.

The ZnO A_1(TO) mode (~380cm^{-1}) can be seen in all samples, although it is weaker in some than others. In figure 3.4 (b) above, the A_1(TO) mode is shown in the Raman spectrum of sample *q*. There is no evidence of the E_2 mode apart from a small

broad peak at ~440cm^{-1} in samples *g*, *h* and *q*. Again this can be seen in fig 3.4 (b) between the peaks labelled 431cm^{-1} and 447cm^{-1}.

3.4 X-Ray Diffraction

3.4.1 Experimental Conditions:

The XRD spectra were taken with a Siemens Diffrac D500 diffractometer in θ-2θ mode. The $K\alpha_1$ line from a Cu source was used. The step size was 0.02^0 for samples *a* and *d* and 0.05^0 for samples *b* and *c* of the ZnO samples.

3.4.2 Zinc Oxide XRD Spectra

The (0002) (~34.5^0) peak and the (0004) (~72^0) peak are indicative of the c-axis being perpendicular to the substrate as they are reflections from the planes that intersect the c-axis at right angles. The peak at approximately 42^0 is from the sapphire substrate. The intensity of the XRD from the film is sensitive to surface roughness and this may cause a reduction in peak height.[7] These ZnO films are estimated to be of the order of 200nm thick, from using a profilometer measurement on a sample with a growth step. All samples are expected to be of the same thickness as the growth time was the same for all.

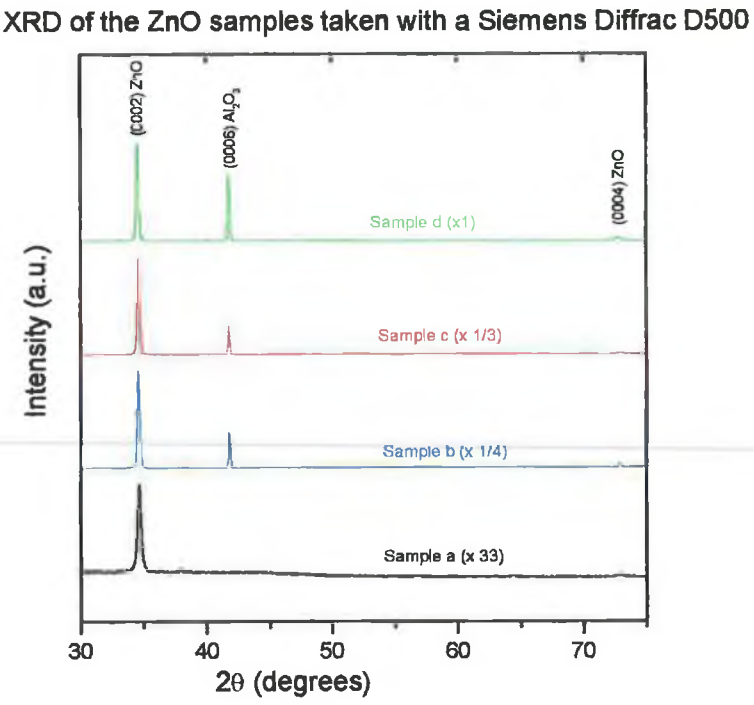

***Figure 3.5**: XRD of samples a, b, c and d.*

While there is some evidence that other reflections exist under magnification (figure 3.6), the XRD data are indicative of highly c-axis oriented material. The small contributions from these planes indicate slightly inferior quality of crystal. Note: a-axis parameters cannot be accurately calculated from these contributions.

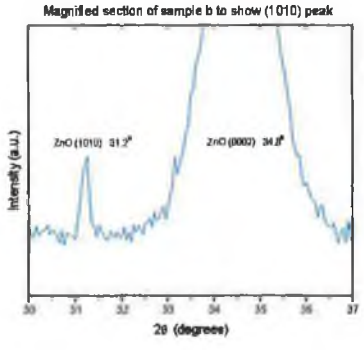

***Figure 3.6**: Close up of XRD of sample b.*

The following table shows the details that the XRD spectra provided through using equations 2.3, 2.4 and 2.5.

sample	Anneal temp (^{0}C)	FWHM (^{0}) of (0002) (corrected)	Average Grain Size (nm)	C-axis lattice length (Å) Using (0002)
a	none	0.261	30.6	5.18
b	400	0.140	52.2	5.18
c	500	0.122	57.7	5.18
d	600	0.119	58.7	5.19

***Table 3.4**: These calculations were performed using the equations given in chapter 2.*

Note: The calculations above were performed using the (0002) peak, as opposed to the (0004) peak which is also visible in the XRD graphs, as the signal to noise ratio of the (0002) peak is much higher. However, the FWHM's of the (0004) in all four graphs follow the same trend as the corresponding (0002) FWHM's.

Of particular interest is that the average grain size of each sample increases upon increasing annealing temperature. This shows that the annealing has a positive, repairing effect on the ZnO grains. Also, although the lattice parameters change little with annealing, the c-axis is shorter than average reported values of ~5.20Å [8]. This indicates a strain along the direction of the a-axis that is probably due to the large lattice mismatch of ZnO with the sapphire substrate.

3.4.3 Manganese-doped Zinc Oxide XRD Spectra

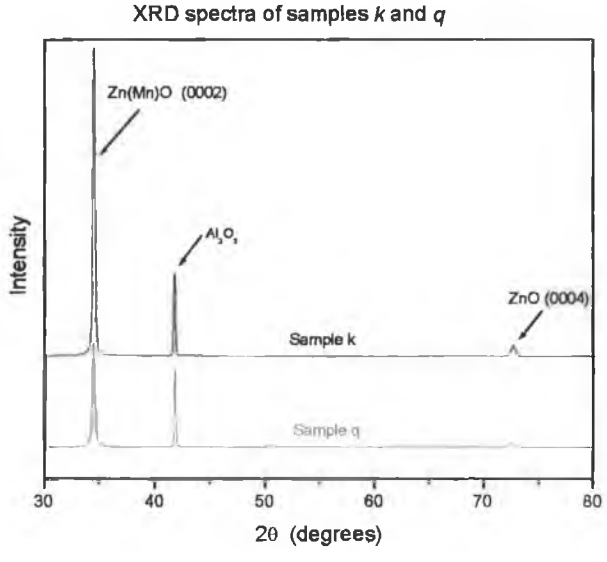

***Figure 3.7**: XRD of samples k and q.*

Figure 3.7 shows the best XRD results. These are taken from samples *j* and *l*. Both samples were grown at relatively high temperatures and both were annealed.
The most important thing to note from these spectra that there are no major contributions from what may be a regular array or plane of Manganese interstitial atoms. This strongly suggests that the Mn atoms occupy the Zn sites. In these two spectra the contribution from the sapphire band is a lot less than in the other XRD results indicating the superior quality of these samples.

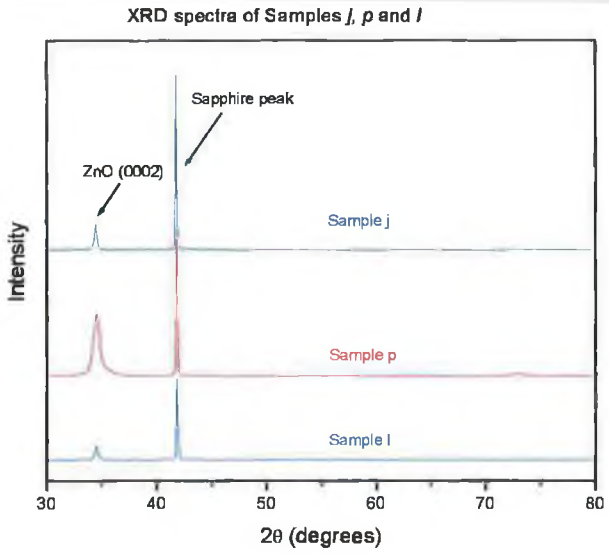

***Figure 3.8**: XRD spectra of samples l, p, and j.*

Figure 3.8 shows the next 3 spectra and these were taken from unannealed samples grown at 400°C and 550°C. In these, the sapphire peak is dominating the spectra and there is likely to be very small contributions from other planes when examined closely. However these spectra are still of superior quality than the spectra below (fig 2.9), which shows XRD of the two samples grown at 250°C. The (0002) peak is of very low intensity and the sapphire dominates the spectra. The reduction in peak height indicates a greater degree of surface roughness.[7]

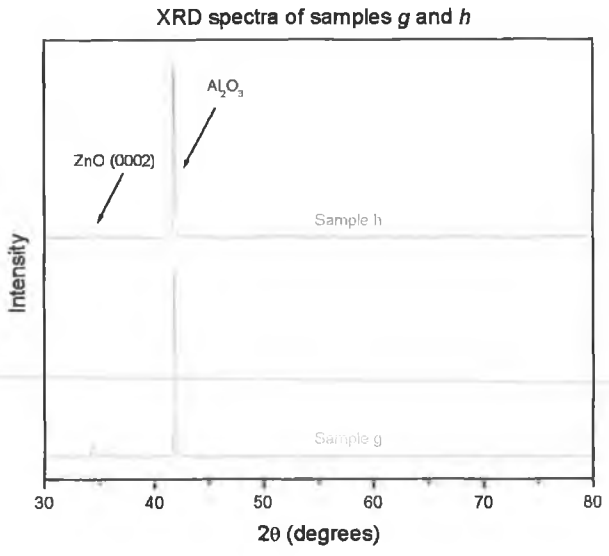

***Figure 3.9**: XRD spectra of samples g and h.*

Note: In the XRD graphs shown figures 3.7, 3.8 and 3.9 the spectra are vertically shifted for clarity.

Table 3.5 shows the calculations made with the results from these spectra. The FWHM have been corrected for instrument broadening and they can be used for comparison purposes.

Sample	Growth temp (^{0}C)	Anneal conditions*	FWHM (B) of (0002) peak (^{0})	Average grain size (nm)	c-axis lattice length (Å) (0002)
g	250	none	0.293	32.3	5.21
h	250	20 mins	0.396	22.5	5.21
j	400	none	0.291	32.6	5.20
k	400	20 mins	0.245	41.4	5.19
l	400	20 mins (noO_2)	0.344	26.5	5.19
p	550	none	0.701	12.2	5.19
q	550	20 mins	0.310	30.1	5.20

***Table 3.5**: Table of average grain sizes and c-axis lengths for $Zn_{0.87}Mn_{0.13}O$.*

* All samples were annealed at their growth temperature and in 0.4 mbar of O_2

Upon examination of the results here, particularly the ZnO/Al_2O_3 ratios, it can been seen that samples grown at 400°C or over and that were annealed in oxygen are of the best crystal quality. This improvement with higher growth temperatures and with anneals, is generally consistent with the ZnO data. The average c-axis length in the $Zn_{0.87}Mn_{0.13}O$ samples is longer than in the ZnO samples, which agrees with the literature that an increase in doping can increase the lattice parameters [9]. Also, the grain sizes are comparable to those of the ZnO samples and there is no evidence in the $Zn_{0.87}Mn_{0.13}O$ samples of grain sizes increasing with growth temperature or anneal conditions. This is an interesting result indicating a different mode of crystal recovery in the $Zn_{0.87}Mn_{0.13}O$ samples compared to the ZnO samples.

3.5 References

1. For example: G.J. Exarhos, S.K. Sharma, Thin Solid Films **270**, 27 (1995) and B.J. Jin, S. Im, S.Y. Lee, Thin solid Films **366**, 107 (2000)
2. T.C. Damen, S.P.S. Porto and B. Tell, Phys. Rev. **142**, 570 (1966)
3. C.A. Arguello, D.L. Rousseau, S.P.S. Porto, Phys. Rev. **181**(3), 1351 (1969)
4. R.C.C Leite, J.F. Scott and T.C. Damen, Phys. Rev. Letters **22**(15), 780 (1969)
5. H. Ibach, Phys Rev. Lett. **24**(25), 1416 (1970)
6. D.L. Peterson, A. Petrou, W. Giriat, A.K. Ramdas, S. Rodriguez, Phys. Rev. B **33**(2), 1160 (1986)
7. B.D. Cullity, Elements of X-Ray Diffraction, Adison-Wesley publishing company Inc. (1978)
8. K.-H. Hellwege (Ed), Numerical Data and Functional Relationships in Science and Technology, Group III: Crystal and Solid State Physics, Volume **17b**, Physics of II-VI and I-VII Compounds, Semimagnetic Semiconductors, Landolt-Bornstein, Springer-Verlag (1982)
9. T. Fukumura, Z. Jin, A. Ohtomo, H. Koinuma, M. Kawasaki, Appl. Phys. Lett **75**(21), 3366 (1999)

Chapter 4: Discussion

4.1 Introduction

The essence of the work is explored in this chapter. First the ZnO Raman results will be discussed. The correlation between the Raman spectra and the XRD spectra along with a consistent interpretation of these data will be presented. The UV resonance spectra will be included in this discussion. Following will be an interpretation of the Raman spectra of the ZnMnO samples, with support from XRD, which was also performed on these samples.

4.2 Zinc Oxide Discussion of Results

In this discussion the ZnO Raman and XRD results are compared and shown to complement each other very well. From these observations certain explanations or models to describe the changes in Raman spectra and hence, crystal structure, are considered.

4.2.1 Correlation of Raman and XRD results

The behaviour of the broad mode at 570cm^{-1} was noted in Chapter 3 but now we will emphasise how its features change with increasing annealing temperature. The unpolarised Raman spectra can been seen again in figure 4.1(b). In samples *a* and *b*, the 570cm^{-1} E_1(LO) mode is two orders of magnitude more intense than in samples *c* and *d*. In samples *a* and *b* it is also very asymmetric, so much so, that from the peak at ~570cm^{-1} its low energy side extends to

~500cm^{-1}. Sample *c* shows considerable changes with increased annealing temperature so that the E_1(LO) mode becomes less asymmetric and less intense. Finally, sample *d*, which was annealed at the highest temperature, shows a symmetric E_1(LO) mode, that has a similar intensity to other peaks in its spectrum.

Taking a closer look, it can be seen that the Raman LO mode behaviour correlates well with the XRD results in terms of grain size calculations. The correlation between the average grain size of each sample and annealing temperature is shown in the graph in figure 4.1 (a). From this graph it can be seen that the grain size increases with annealing temperature up to 600°C. This increase in grain size means that the crystal structure is being repaired with annealing.

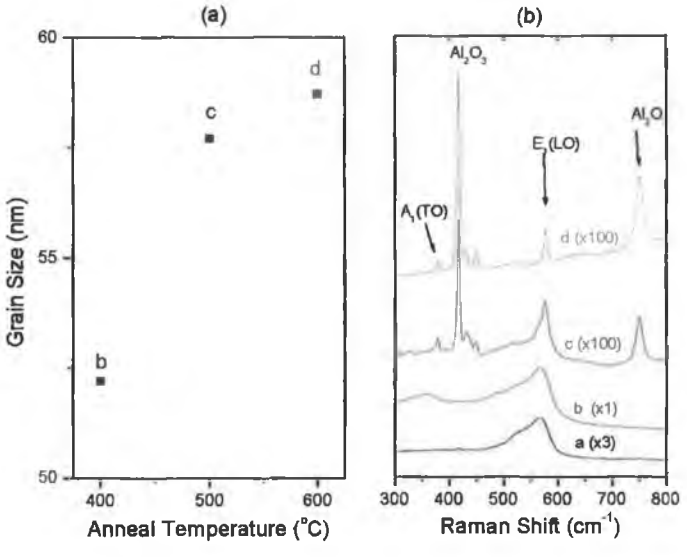

***Figure 4.1**: (a)Graph of grain sizes v anneal temperature shows an approximately linear relationship and (b) Non-resonant Raman spectra of ZnO samples.*

In summary, as the grain size increases, from samples *a* to *d*, with annealing temperature, the intensity, asymmetry and FWHM of the 570cm^{-1} band in the Raman spectra decreases. This band has often been reported in ZnO Raman and has consistently indicated inferior crystal quality [1], [2].

4.2.2 Explanations of Results

These has been many suggestions proposed to explain the 570cm^{-1} mode's enhancement and asymmetry including (i) contributions from both A_1(LO) and E_1(LO) modes due to random crystallite orientation,[1] (ii) contributions from plasmons coupled to the (zone centre) LO modes,[2], [3] (iii) resonance enhancement due to impurities in the bandgap[1] and (iv) Electric Field Induced (EFI) Raman enhancement of LO modes[2], [3] and the presence of surface, local and gap modes.[2], [5], [6] We will discuss these various explanations and their merits and deficiencies in order.

(i) A_1(LO) Mode Contribution

When the A_1(LO) mode is present in a ZnO Raman Spectrum, it appears at a wavenumber lower, but close, to that of the E_1(LO) mode according to previous experimental results. The splitting of the LO mode into A_1 and E_1 components is due to the fact that electrostatic forces dominate over the anisotropy of the crystal.[7] The first explanation above accounts for the low energy asymmetric side of the E_1(LO) mode by saying that it can be caused by contributions from the A_1(LO) mode phonon. In order that there be contributions from A_1(LO) and E_1(LO) modes, the crystallites would have to be very randomly oriented, some with c-axis perpendicular to the substrate (to see E_1(LO) mode contributions) and some with c-axis parallel to the substrate (to see A_1(LO) mode contributions). The effects of annealing would then be to re-orientate the crystal planes contributing to the A_1(LO) mode so that it would disappear, leading to a symmetric E_1(LO) mode peak.

However the XRD results rule this out. Firstly, the un-annealed sample shows negligible contributions from other crystal planes. This indicates that the A_1(LO) mode is not present even before annealing*. Secondly, the (0002) peak positions remain unchanged upon annealing.

* In the Raman Experimental conditions used to obtain the results presented here the A_1(LO) mode should not be present. If the experimental configuration was changed it would be possible to see this mode using the same samples.

This means there has been no significant reorientation of crystallites upon annealing. (Note that the (0002) peak is indicative of c-axis being perpendicular to the substrate.)

Another argument against the idea of A_1(LO) mode contributions is that it does not reasonably account for the dramatic intensity decrease of the 570cm^{-1} mode with annealing temperature.

(ii) Coupled Phonon-Plasmon Modes

The second explanation deals with the relationship between the LO modes and the free carrier concentration in the crystal. The LO modes have been known to couple with plasmons in the crystal bulk.[8] It has been well reported that the intense, asymmetric LO band occurs when the free carrier concentration is high as in doped ZnO[2], [3], [9] or undoped oxygen deficient ZnO[1] and that its intensity reduces upon annealing in oxygen in the latter case.

The effect of high free carrier concentration and mobility causes the appearance of coupled phonon-plasmon modes. Only the LO phonon mode couples with plasmons due to their common longitudinal electric fields. This leads to two coupled modes L^+ and L^-. According to Tzolov et al. [2] in the case of ZnO and Rai et al. [8] in the case of ZnSe, the L^- mode can account for the low frequency shoulder of the LO mode as its intensity is of the same order as the enhanced LO peak.[2] However the coupling of the L^- mode only occurs when there are free carriers of high mobility in the material (note: the PLD ZnO samples are highly polycrystalline and hence would have low mobility).[10] Since the carrier concentration and mobility needs to be significant and there is no evidence of an L^+ mode at frequencies higher than the Longitudinal Optical phonon modes, it is unlikely that LO phonon-plasmon coupling causes the enhancement and a-symmetry here.[10], [11]

(iii) Resonantly Enhanced Impurities

The third theory put forward suggests that the E_1(LO) mode may be resonantly enhanced due to impurity levels in the band gap. The idea is that the impurities create new electronic levels in the band gap with which the incident

radiation corresponds to and as explained in section 2.4.2, this can cause resonance enhancement of LO modes. Resonance enhancement due to impurities could indeed account for the extremes in the E_1(LO) mode intensity from samples *a* to *d*. When annealed, the impurities would be annealed out of the samples leaving no impurity levels in the bandgap. In turn, the E_1(LO) mode in samples *c* and *d* would not be resonantly enhanced and therefore their intensities would greatly reduced.

The UV Raman spectra, in Figure 3.2, are shown to demonstrate resonance Raman enhancement. The two chosen are taken from samples *a* and *c*. This is to show that although samples *a* and *c* show considerably different XRD and non-resonant Raman results their Resonance Raman spectra are very similar.

However, we feel that resonantly enhanced LO modes cannot account for the asymmetry of the E_1(LO) peak. From the (purposely) resonant Raman spectra of figure 3.2, the LO mode can be seen to be very symmetric when resonantly enhanced. Furthermore, the presence of second, third and higher orders are characteristic of resonant Raman spectra. There is no sign of higher orders of the E_1(LO) mode at frequencies corresponding to its second, third and higher order modes in these Raman spectra.

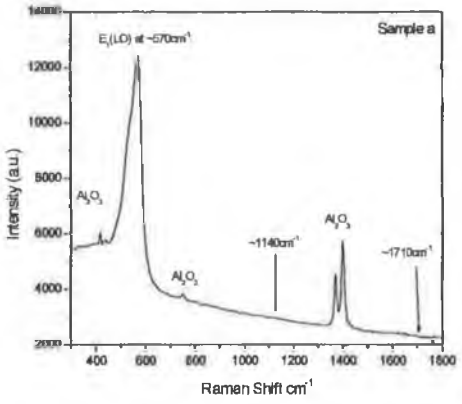

***Figure 4.2**: Non-resonant Raman spectrum of sample a extended to show that no impurity resonantly enhanced second order LO modes are present.*

Second and third orders would occur at frequencies of 1140cm^{-1} and 1710cm^{-1} respectively and are not present, as can be seen from the extended spectrum of sample *a* in figure 4.2.

(iv) EFI Enhancement and Surface, Local and Band Modes

Returning to the excellent correlation between the XRD and Raman spectra brings up the situation involving localised or surface phonon modes and EFI Raman Scattering.

In a finite sample the bulk phonon modes change according to the size and shape of the crystal. Surface phonon modes occur when the sample is small or thin enough, i.e. if the sample is considerably smaller than the wavelength of the incident radiation.[12] Our ZnO samples have average grain sizes of ~ 50nm (average over all four samples) compared with incident radiation of 633nm giving the conditions necessary to produce surface phonon modes.

Localised, gap and band phonon modes can occur due to lattice defects and vacancies[13], in this case caused by grain boundaries, where there is a break in the translational symmetry of the crystal, and by a small contribution from oxygen vacancies.[14] In samples *a* and *b* the small grain size and large concentration of grain boundaries can cause localised modes that could reasonably account for the low energy side of the E_1(LO) mode.

Tzolov et al.[2] and Ibach [15] have reported surface and localised (strictly band modes) phonon modes at 468cm^{-1} and 516 cm^{-1} and 543cm^{-1} and 553cm^{-1} respectively. It is important to note that these wavenumbers fall into the range of the broad, low energy side of the E_1(LO) mode.

The affect of annealing the samples is to restore the translational symmetry, increase the average grain size of the samples i.e. annealing affects all the conditions necessary for the production of surface and local phonon modes. We feel this is what has happened in sample *c* and to a greater extent in sample *d*. The result is no surface, local or band modes to cause the low energy side of the E_1(LO) mode. (Refer to figure 3.1 or 4.1 (b) to observe this reduction in asymmetry.)

The presence of surface and local modes reasonably accounts for the asymmetry of the E_1(LO) mode in samples *a* and *b* and we will now explore the possible mechanism behind its intensity enhancement.

The intensity enhancement of the LO peak is thought to be due to Electric Field Induced Raman scattering. The electric field is set up due to charge trapping at grain boundaries[16].

The following band diagrams can help explain the mechanism for the production of an Electric field in the grains:

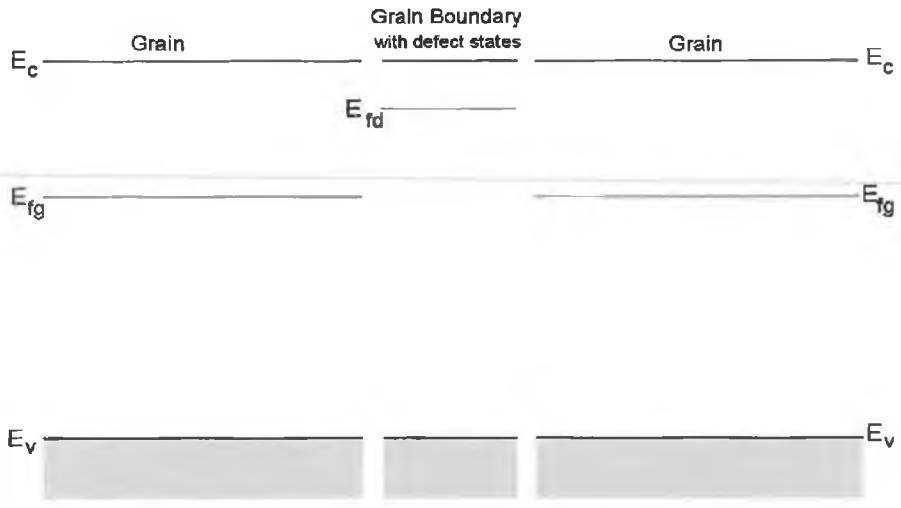

***Figure4.3**: Band diagram of two grains and the electronic state of their boundary before joining. In figure 4.2, E_c and E_v are the positions of the conduction band and valence band respectively, E_{fg} is the Fermi level in the grains and E_{fd} is the Fermi level in the boundary.*

Consider the band diagram in figure 4.3. The first stage of this process is the trapping of free electrons.

Due to the discontinuity of the lattice structure at the grain boundaries, defect states or defect energy levels occur. These defect states trap free charges and so deplete the bulk of the grains of, in this case, electrons. A depletion layer is formed in the grains because there are no free carriers left.

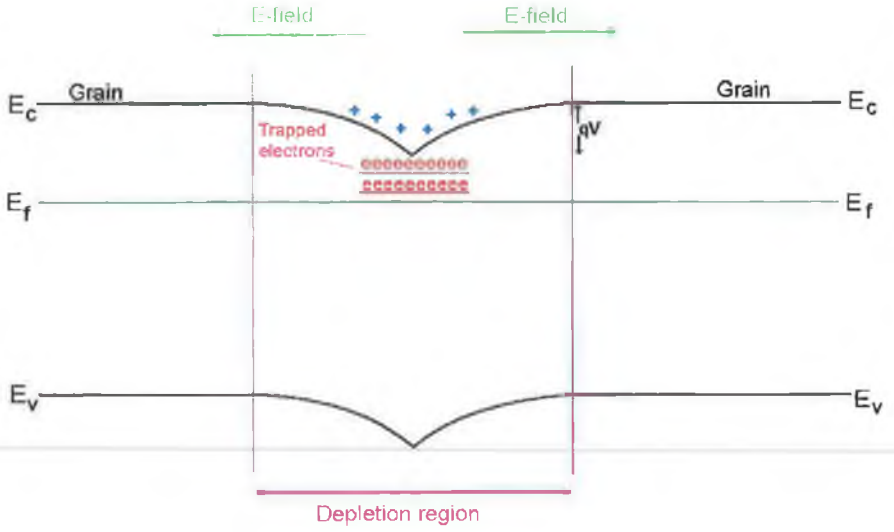

***Figure 4.4**: The formation of the E-field after the two grains have joined. In figure 4.4, The electrons are indicated by 'e'. E_c and E_v are as in figure 4.2. E_f is the Fermi level through the whole structure. The pink arrow indicates the depletion region width and qV is the potential barrier height.*

Eventually there is a local build up of negative (or positive) charge and this naturally causes an electric field. This is shown in figure 4.4. Once formed, this electric field causes the enhancement of the LO mode by altering the polarisibility tensor and hence the scattering efficiency of the mode as explained below.

The induced dipole moment responsible for Rayleigh and Raman scatter was previously given by equation 2.14.

$$\mu = \alpha_0 E_0 Cos2\pi\nu t + \frac{r_0 E_0}{2}\left(\frac{\partial\alpha}{\partial r}\right)\left[Cos2\pi(\nu-\nu_p)t + Cos2\pi(\nu+\nu_p)t\right]$$

Vibrational Raman scatter is based on a significant displacement of the polarisibility tensor, α, with respect to the vibrational co-ordinate system, r, i.e. the term $\left(\frac{\partial\alpha}{\partial r}\right)$ in equation 2.14. This means the larger the displacement, or

$\left(\frac{\partial \alpha}{\partial r}\right)$, the larger the scattering intensity. The (longitudinal) Electric field that is set up in the grains, increases the periodic distortion of the polarisibility tensor associated with the LO modes, before interaction with incident electromagnetic radiation occurs. The electric field of the incident radiation then displaces the tensor components from *r* even more, increasing scattering efficiency and hence the intensity of the LO mode(s).

For samples with small grain size, trapping is abundant, as there is a greater concentration of grain boundaries and defects. A large E-field is set up and scattering is enhanced. In annealed samples the grain size has increased so that charge trapping lowers and the grain boundary density is reduced. In this case, the E-field is very small and little or no enhancement occurs. Similar effects are seen in the Photoluminescence spectra of ZnO polycrystalline samples. [17]

4.2.3 Conclusions

In conclusion, a number of explanations have been considered for the possible cause of the extreme intensity and asymmetry of the E_1(LO) mode in samples *a* and *b* compared with the samples annealed at higher temperatures, *c* and *d*. The dominant physical aspect of increasing average grain size with annealing temperature has been considered in most of the proposed explanations. However, the final model is believed to comprehensively describe the changes that the Raman spectra, the XRD and the samples undergo with increasing anneal temperature.

4.3 Manganese-doped Zinc Oxide Discussion of Results

Originally, the study of growth temperature and annealing effects was the aim of the preliminary study for the $Zn_{0.87}Mn_{0.13}O$ samples. However, although the $Zn_{0.87}Mn_{0.13}O$ samples were grown at a range of temperatures and underwent varied anneal conditions, the structure of their Raman spectra remained very similar. The similarities are evident from the two broad spectral features centred around 435cm^{-1} and 590cm^{-1} in almost all samples, and the detail that occurs on the low energy side of the E_1(LO) phonon mode as explained in the results section 3.3.3.

4.3.1 Explanation of Results

The main point of note is that there is a substantial difference between the non- resonant Raman spectra of ZnO and $Zn_{0.87}Mn_{0.13}O$. The $Zn_{0.87}Mn_{0.13}O$ spectra are not greatly affected by the annealing and growth conditions. The most obvious difference is that there is no evidence of Electric Filed Enhancement (EFI) of the E_1(LO) mode in $Zn_{0.87}Mn_{0.13}O$ even though the grain sizes are comparable with those of the ZnO samples, *a* and *b*. It is possible that the Mn doping causes this, by substantially increasing carrier concentration and therefore, increasing screening effects.

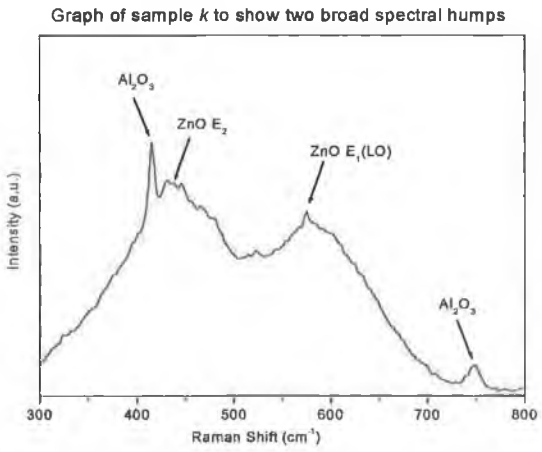

***Figure 4.5**: Note the two broad spectral features.*

The origin of the two broad features centred on 435cm^{-1} and 590cm^{-1}, and shown for sample *k* in Figure 4.5, is unclear. Again, since these structures are not present in ZnO samples, it is reasonable to suggest that they are due to the introduction of manganese into the lattice. Similar peaks have been reported as being due to an Mn-O stretching bond [18]. Although Mn-O stretching bonds are not present in crystalline wurzite $Zn_{(1-x)}Mn_xO$, they may appear here, with a broadened distribution, due to the range of local environments in the polycrystalline material.

The detail of small peaks that occur in the range 500cm^{-1} to 600cm^{-1} (as examined in section 3.3.3) could be due to intermediate phonon mode behaviour combined with the presence of surface phonon modes (the possibility that they are related to surface modes is strengthened by the relatively small grain sizes in these samples). The intermediate mode theory (as described by the Random Element Isodisplacement (REI) model [19]) describes the presence of TO and LO modes which are present in Raman spectra due to the transition of the $Zn_{(1-x)}Mn_xO$ compound between ZnO and MnO with increasing x. The complexities of analysis of intermediate modes would ideally involve the use of polarised Raman spectra and samples with varying levels of Mn, i.e. varying values of x. Therefore, our spectra cannot be used for a full development of this theory but they can be roughly compared with other studies.[20], [21]

The XRD spectra show an increase in crystal quality with higher growth/ anneal temperatures, which is maintained in the increase of the XRD peak height

(interpreted to be a reduction in surface roughness). This mode of crystal recovery is very different to the substantial grain growth seen for the ZnO samples and the reasons for this are not clear. Perhaps the manganese stabilises the grains in some way.

The $Zn_{0.87}Mn_{0.13}O$ Raman spectra pose many questions but the main piece of information that can be extracted from the XRD results is that the peak positions of the $Zn_{0.87}Mn_{0.13}O$ XRD do not change compared with the XRD of ZnO. Also, the same ZnO $E_1(LO)$ and $A_1(TO)$ modes are present in the Raman spectra of most $Zn_{0.87}Mn_{0.13}O$ samples. Combining these facts from the XRD and Raman spectra, it can be said that the Mn atoms generally occupy Zn sites in the lattice. Since Mn and Zn have quite similar atomic masses this would be expected. It can be concluded that for a doping levels of Manganese with x = 0.13, the original ZnO wurzite structure does not change.

4.3.2 Conclusions

Form this preliminary study not many conclusions can be drawn except to say that the Mn atoms seem to have a definite effect on the ZnO according to Raman spectra. However, apart from slightly increasing the c-axis lengths, the introduction of x=0.13 manganese into ZnO does not change the compound's structure. Further work is needed for a comprehensive analysis of the effects of manganese doing in ZnO.

4.4 References

1. G.J. Exarhos, S.K. Sharma, Thin Solid Films **270**, 27 (1995)
2. M. Tzolov, N. Tzenov, D. Dimova-Malinovska, M. Kalitzova, C. Pizzuto, G. Vitali, G. Zollo, I. Ivanov, Thin Solid Films **379**, 28 (2000)
3. G.J. Exarhos, A. Rose, C.F. Windisch Jr., Thin Solid Films **308-309**, 56 (1997)

4. W. Richter, M. Shand, E. Burstein, J. Gay, in M. Balkanski (Ed.), Light Scattering in Solids, Flammarion Science, 39 (1971)
5. M.C. Klein, F. Hache, D. Ricard, C. Flytzanis, Phys. Rev. B **42**(17), 11123 (1990)
6. D.S. Chuu, C.M. Dai, W.F. Hsieh, C.T. Tsai, J. Appl. Phys **69**(12), 8402 (1991)
7. C.A. Arguello, D.L. Rousseau, P.S. Porto, Phys. Rev. **181** (3), 1351 (1969)
8. B.K. Rai, R.S. Katiyar – K. Chen, A. Burger, J. Appl. Phys. **83**(11), 6011 (1998)
9. G.J. Exarhos, A. Rose, L.Q. Wang, C.F. Windisch Jr., J. Vac. Sci. Technol. A **16**(3), 1926 (1998)
10. D. Olego, M. Cardona, Phys. Rev. B **24**(12), 7217 (1981)
11. M. Herms, G. Irmer, J. Monecke, O. Oettel, J. Appl. Phys. **71**(1), 432 (1992) Barimov
12. P.M.A. Sherwood, Vibrational Spectroscopy of Solids, Cambridge University Press (1972)
13. J.H. Weiner, W.F. Adler, Phys. Rev. **144**(2), 511 (1966)
14. S.Perkowitz, Optical characterisation of semiconductors, Academic Press Ltd. (1993)
15. H. Ibach, Phys. Rev. Letters **24**(25), 1416 (1970)
16. T.L. Tansley, D.F. Neely, Thin Solid Films **121**, 95 (1984)
17. K. Vanheusden et al., J. Appl. Phys. **79,** 7983 (1996)
18. M.N. Iliev, M.V. Abrashev, H.-G. Lee, V.N. Popov, Y.Y. Sun, C. Thomsen, R.L. Meng, C.W. Chu, Phys. Rev. B **57**(5), 2872 (1998)
    A.E. Pantoja, H.J. Trodahl, A. Fainstein, R.G. Pregliasco, R.G. Buckley, G. Balakrishnan, M.R.Lees, D. McK. Paul, Phys. Rev. B **63**(13) 132406 (2001)
19. L. Genzel, T.P. Martin, C.H. Perry, Phys Status Solidi B **62**, 83 (1974)
20. D.L. Peterson, A. Petrou, W. Giriat, A.K. Ramdas, S. Rodriguez, Phys. Rev. B **33**(2), 1160 (1986)
21. E.-K. Suh, Akhilesh K. Arora, A.K. Ramdas, S. Rodriguez, Phys. Rev. B **45**(7), 3360 (1992)

Chapter 5: Conclusions and Future Work

5.1 Conclusions

The aim of this project was to examine ZnO thin films grown by PLD and by using Raman spectroscopy and XRD, determine how the growth parameters affected film quality. As a secondary part, a preliminary study of $Zn_{(1-x)}Mn_xO$ was also carried out with the same aim in mind.

Under the particular growth conditions used to grow the ZnO samples studied here, it was found that annealing ZnO samples in O_2 directly after deposition, at a temperature higher than the growth temperature, has a positive effect on crystal structure and hence, quality. This was shown through Raman spectroscopy and XRD whose combined results revealed that the average grain size of ZnO samples was increased under these annealing conditions, leading to lower grain boundary density, reduced charge trapping and improved crystal structure.

A model was proposed which consistently explains the correlation between XRD and Raman spectroscopy. Both methods complemented each other very well and with a third parameter, anneal temperature, created interesting questions, which led to a variety of explanations from which conclusions about the samples were drawn.

For the purposes of this study Pulsed Laser Deposition was shown to be very suitable for the growth of highly oriented ZnO thin films. The actual deposition was very fast (~20mins) and changing oxygen partial pressure, substrate temperature or target to substrate distance could be done easily and independently of adjusting other parameters. PLD suits growing sets of samples, like those used in this study, on small substrate sizes, using small amounts of the target material.

$Zn_{0.87}Mn_{0.13}O$ was successfully grown by PLD. $Zn_{0.87}Mn_{0.13}O$ Raman spectra still maintained most of the ZnO characteristics along with some unusual features. As it was a preliminary study no definite conclusions can be drawn about these features, although it is speculated that the unusual amount of detail in the area of the ~570cm^{-1} ZnO E_1(LO) mode is likely to be due to an intermediate mode behaviour – i.e. that some peaks are due to ZnMn bonds and some due to MnO bonds. The Raman spectra again correlate well with the XRD in these samples to show that the Manganese atoms generally sit on Zinc atom sites in the lattice.

Finally, as it was shown that in-situ annealing of $Zn_{0.87}Mn_{0.13}O$ at the growth temperature has a different effect on sample quality than ZnO. The effect on $Zn_{0.87}Mn_{0.13}O$ of in-situ annealing at temperatures higher than the growth temperature should be examined.

5.2 Future Work

The overall aim of the group project is to obtain lasing action from ZnO, and to reach that objective good quality films are needed, both structurally and optically. This project has identified that with current growth parameters, maybe longer annealing times should be considered to improve the quality of the films. Apart from that, sets of samples with varying oxygen partial pressures, varying target substrate distances and varying substrate temperatures would be areas to look at and test for quality.

Another major area of concern in PLD grown ZnO samples is the consistent oxygen deficiency. Growing ZnO in other gases, such as N_2O, or creating an oxygen rich target may combat this problem.

For $Zn_{0.87}Mn_{0.13}O$ it is suggested that a full study should be carried out with different levels of Mn in the $Zn_{(1-x)}Mn_xO$. Much more about the effects of Mn could be told from a study of this type, for example, at what Mn doping level will the wurzite structure change? If polarisation studies were carried out would the two

spectral features be direction dependent i.e. related to a particular type of mode? Since not much has been published on the Raman scattering of $Zn_{(1-x)}Mn_xO$ the area is wide open for a large range of fundamental studies.

Since manganese doping increases the bandgap in most II-VI's such as $Zn_{(1-x)}Mn_xO$, short wavelength emission from this material could also be investigated.